SEGMENTAL MULTI-POINT LINEARIZATION FOR TOPOLOGY OPTIMIZATION AND RELIABILITY ANALYSIS

BY

KE LIU

THESIS

Submitted in partial fulfillment of the requirements
for the degree of Master of Science in Civil Engineering
in the Graduate College of the
University of Illinois at Urbana-Champaign, 2014

Urbana, Illinois

Advisers:

Professor Glaucio H. Paulino
Professor Paolo Gardoni

ABSTRACT

This paper proposes an efficient gradient-based optimization algorithm to solve reliability-based topology optimization (RBTO) of structures under loading and material uncertainties. Topology optimization is a powerful design tool as it can provide the most efficient material layout for structural design problems under given conditions and limitations. However, most attempts are formulated in a deterministic manner, which may be impractical as this formulation ignores the inherent uncertainty and randomness in structural design problems. The objective of RBTO considered in this research is to identify the optimal topology of truss structures with minimum weight which also satisfy certain requirements on the reliability of the structures. As a subtopic of reliability-based design optimization (RBDO), RBTO problems are primarily performed with algorithms based on a first-order reliability method (FORM) which are well developed in the literature for RBDO. However, those algorithms may lead to deficient or even invalid results for RBTO problems since the gradient of probabilistic constraint, calculated by first order approximation, is not accurate enough for RBTO to converge correctly regardless of how accurate the failure probability is approximated. A segmental multi-point linearization (SML) method is proposed for a more accurate estimation of failure probability and its gradient. Numerical examples show that the RBTO algorithm based on the SML is more stable numerically and is able to converge to a solution that is closer to the true optimum than conventional FORM-based algorithms. The obtained optimal topology can serve as a starting point for engineers to make the design of structures both economic and reliable.

To my parents, for their unconditional love and support.

ACKNOWLEDGEMENTS

First and foremost, I would like to express my profound gratitude to my advisors, Professor Glaucio H. Paulino and Professor Paolo Gardoni. Without their trust, patient guidance, and encouragement through the process of this master thesis, this work would never have been accomplished. I am inspired by their enthusiasm to research, attention to detail, and their dedication to the profession. I feel that I have learned a lot from them.

I greatly appreciate my colleagues, Cameron Talischi, Arun Gain, Tomas Zegard, Sofie Leon, Daniel Spring, Junho Chun, Evgueni Filipov, Heng Chi, Xiaojia Zhang, Tuo Zhao, Maryam Eidini, Adeildo Soares Ramos Jr., Luis Arnaldo, Peng Wei, Armin Tabandeh, Roberto Guidotti, Hao Xu, Andrea Brignone, Marco Andreini, for always being helpful and supportive during my graduate study. Being along with them helps me to learn how to become professional in my academic life. Special thanks are due to Junho Chun and Armin Tabandeh, who denote their time to help me revise and polish the thesis.

In addition, I would like to thank all of my friends. Although many of them are on the other side of the Pacific Ocean, they all give me close support.

The author also wants to acknowledge the courtesy from Dr. Svanberg for the MATLAB code of MMA.

I am grateful for the financial support from National Science Foundation through the research grant 1234243.

Finally, and most importantly, I wish to thank my parents, Tianxiong Liu and Wenhong Zhang. All of my accomplishment and success should owe to my parents. No words can describe how I appreciate them for what they have done for me.

TABLE OF CONTENTS

LIST OF TABLES vii

LIST OF FIGURES viii

LIST OF ABBREVIATIONS x

NOMENCLATURE xi

CHAPTER 1 **INTRODUCTION** 1
1.1 Motivation 1
1.2 Thesis Organization 3

CHAPTER 2 **GROUND STRUCTURE APPROACH** 4
2.1 Nested Formulation 4
2.2 Sensitivity Analysis of Compliance 7

CHAPTER 3 **RELIABILITY-BASED DESIGN OPTIMIZATION** 9
3.1 Reliability Methods 9
3.2 A Review of RBDO Approaches 12
3.3 Gradient of Probability Function 15

CHAPTER 4 **RELIABILITY-BASED TOPOLOGY OPTIMIZATION FORMULATION** 21
4.1 Segmental Multi-Point Linearization for Sensitivity Calculation 22
4.2 Improvement of Reliability Assessment 27
4.3 SML-Based RBTO Algorithm 29

CHAPTER 5 **NUMERICAL EXAMPLES** 33
5.1 A Benchmark Problem 33
5.2 Symmetric Crane Arm Design 34
5.3 Unsymmetric Crane Arm Design 40
5.4 T-shaped Building Design 43

CHAPTER 6 **CONCLUDING REMARKS AND SUGGESTIONS FOR FUTURE WORK** 47
6.1 Contributions 48
6.2 Suggestions for Future Work 48

REFERENCES 49

LIST OF TABLES

5.1 Statistics of Random Variables for Example 4. 44

LIST OF FIGURES

2.1 The four levels of the ground structure on a 4×4 grid. (a)Level 1: 72 non-overlapping members. (b)Level 2: 120 non-overlapping members. (c)Level 3: 176 non-overlapping members. (d)Level 4: 200 non-overlapping members. 5

3.1 Illustration of FORM and SORM. 11
3.2 Trajectory of the optimization process of RIA and PMA in the standard normal random space. 13
3.3 Geometric representation of general continuous limit state surface. 16
3.4 Geometric representation of affine limit state surface. 18

4.1 Graphical illustration of the proposed segmental multi-point linearization method (SML), where green triangle refers to the reference point, blue circles refer to sample point, $(\pm i)$ represent $\mathbf{u}^{(\pm i)}$. 23
4.2 Parabolic limit state function. 26
4.3 Comparison of approximations of sensitivity. 28
4.4 SML for parabolic limit state surface. 28
4.5 Comparison of approximations of failure probability. 29

5.1 Benchmark problem for RBTO. (a) Domain, loading and boundary conditions. (b) Optimal topology. 33
5.2 Design domain and boundary conditions of example 2. 35
5.3 Ground structure used to do RBTO which has 440 non-overlapping members. 36
5.4 Optimal topology by DTO. 37
5.5 Optimal topology by FORM-based PMA. 37
5.6 Contour plot of $G(\mathbf{u}, \mathbf{x}^*)$ for optimal design of Fig. 5.5. The blue circle indicates the design point computed by the PMA; the green triangle refers to the actual position of design point; the red solid curve is the limit state surface described by $G(\mathbf{u}, \mathbf{x}^*) = 0$. 37
5.7 Another optimal topology by FORM-based PMA. 38

5.8 Optimal topology by SML-based RIA taking design point the reference point. 38
5.9 Optimal topology by SML-based RIA enforcing reference point to be on the line $u_1 = u_2$. 38
5.10 Contour plot of $G(\mathbf{u}, \mathbf{x}^*)$ for optimal design of Fig. 5.8. The blue circle indicates the sample points; the green triangle refers to the design point(s); the green triangle refers to the actual position of design point; the red solid curve is the limit state surface described by $G(\mathbf{u}, \mathbf{x}^*) = 0$. 39
5.11 Contour plot of $G(\mathbf{u}, \mathbf{x}^*)$ for optimal design of Fig. 5.9. The blue circle indicates the sample points; the green triangle refers to the design point(s); the green triangle refers to the actual position of design point; the red solid curve is the limit state surface described by $G(\mathbf{u}, \mathbf{x}^*) = 0$. 40
5.12 Design domain and boundary conditions of example 3. 41
5.13 Optimal topology by DTO. 41
5.14 Optimal topology by FORM-based PMA. 41
5.15 Optimal topology by SML-based RIA with design point being the reference point. 42
5.16 Contour plot of $G(\mathbf{u}, \mathbf{x}^*)$ for optimal design of Fig. 5.15. The blue circle indicates the sample points; the green triangle refers to the design point; the red solid curve is the limit state surface described by $G(\mathbf{u}, \mathbf{x}^*) = 0$. 43
5.17 Probability distribution of Young's modulus E. 44
5.18 Optimal topology by SML-based RIA considering randomness of E. 44
5.19 T-shaped building design. (a) Domain, loading and boundary conditions. (b) Ground structure used to perform RBTO which contains 526 non-overlapping members. 45
5.20 Optimal topology by DTO. 45
5.21 Optimal topology by SML-based RIA on the ground structure shown in Fig. 5.19b. 46
5.22 Optimal topology by SML-based RIA on a refined ground structure with 26180 members. 46

LIST OF ABBREVIATIONS

FORM	First Order Reliability Method
SORM	Second Order Reliability Method
MCS	Monte Carlo Simulation
PDF	Probability Density Function
CDF	Cumulative Distribution Function
DTO	Deterministic Topology Optimization
RTO	Robust Topology Optimization
RBDO	Reliability-Based Design Optimization
RBTO	Reliability-Based Topology Optimization
CRBTO	Component Reliability-Based Topology Optimization
SRBTO	System Reliability-Based Topology Optimization
C.C.	Correlation Coefficient(s)
SML	Segmental Multi-Point Linearization
MMA	Method of Moving Asymptote
SLP	Sequential Linear Programming
CONLIN	Convex Linearization Method
RIA	Reliability Index Approach
PMA	Performance Measure Approach
MTOP	Multiresolution Topology Optimization
MPP	Most Probable Point

NOMENCLATURE

$\mathbf{x}$	Design variables (i.e. member areas)
$\mathbf{v}$	Original random variables
$\mathbf{u}$	Transformed random variables
$\boldsymbol{\rho}$	Density of members
$\mathbf{b}$	Volume of members
V	Weight of structure; volume of structure if $\boldsymbol{\rho} = \mathbf{1}$
$\mathbf{d}$	Nodal displacement
$\mathbf{F}$	Load vector
$\mathbf{l}$	An artificial vector of weights
C	$\mathbf{l}^{\mathrm{T}}\mathbf{d}$; total compliance of structure if $\mathbf{l} = \mathbf{F}$
$\mathbf{K}$	Global Stiffness matrix
$\mathbf{K}_j^0$	Constant element stiffness matrix
C^{max}	Threshold on compliance
$\mathbf{x}_{min}$	Lower bounds of member areas
$\mathbf{x}_{max}$	Upper bounds of member areas
$g(\mathbf{v})$	Limit state function in original random space
$G(\mathbf{u})$	Limit state function in standard normal space
m	Number of design variables
n	Number of random variables
P_f	Failure probability

P_f^t	Target failure probability
$I(\mathbf{v})$	Indicator function
$\mathbf{u}^*$	Design point
$\mathbf{u}^t$	Most probable point
$\varphi(\cdot)$	Standard normal PDF
$\varphi_n(\cdot)$	n-variate standard normal PDF
$\Phi(\cdot)$	Standard normal CDF
$\Phi_n(\cdot)$	n-variate standard normal CDF
β	Reliability index
β_1	Reliability index approximated by FORM
β^t	Target reliability index
λ, γ_i	Lagrange multipliers
$f(\mathbf{x})$	Objective function of RBDO
$\mathbf{h}(\mathbf{x})$	Equality constraints of RBDO
S	Limit state surface
T	Probability preserving transformation of random variables
$\mathbf{Q}$	Rotational matrix
$\mathbf{R}$	The constant rotational matrix used in SML
p	Number of sample points in SML
$\mathbf{u}^{(+i)}/\mathbf{u}^{(-i)}$	Sample point on the positive/negative part of axis i
$\tilde{\beta}$	Approximation of reliability index
r	Radius of search region
$\mathbf{e}$	Unit vector of axis direction
α	Step size in optimization

CHAPTER 1

INTRODUCTION

1.1 Motivation

Topology optimization allows engineers to design structures that possess most efficient use of material with desired structural behavior. In recent years, as a popular research topic, topology optimization has been applied to engineering problems in a wide range of fields, for example, building design, vehicle design, and human facial reconstruction [1, 2, 3]. Most of the research has been formulated in a deterministic manner, however, deterministic topology optimization (DTO) has limited use for realistic design problems where the inherent uncertainties in loading conditions, material properties and manufacturing process cannot be neglected. There are three main strategies to address this concern, namely robust topology optimization (RTO), model updating, and reliability-based topology optimization (RBTO) [4]. The goal of the RTO is to find a structure that is relatively insensitive with respect to uncertainties in design conditions [5, 6]. Model updating is usually performed with evolutionary algorithms which employ a large number of simulations to identify the best solution(s) to a structural design problem and is often formulated as multi-objective optimization [7, 8]. On the other hand, RBTO aims to manage the effect of uncertainties on structural performance in terms of failure probability during topology optimization process. The advantage of the RBTO is that it allows a quantitative control over the uncertainties, which follows modern design philosophy, while requiring relatively low computational cost. The RBTO is performed at two levels: component reliability-based topology optimization (CRBTO) which considers each failure mode individually, and system reliability-based topology optimization (SRBTO) which deals with a combination of failure modes simultaneously. In this research, we focus on the CRBTO for truss layouts with random loads

and material properties.

The truss layout optimization is performed using a ground structure approach, where the optimal layout of a truss structure is extracted from a very dense set of potential joints and bars by sizing the members and allowing them to vanish [9, 10, 11, 12]. Another popular approach of topology optimization, called density approach, aims to find the best material distribution within a continuum [2, 13]. An important motivation of using the ground structure approach is that it provides directly the truss layout on a base grid so that it is particularly applicable for design of modular space structures [14]. A so-called nested formulation [15] of the ground structure approach is implemented in our RBTO algorithm.

As a design problem, the RBTO can be regarded as a subtopic of a reliability-based design optimization (RBDO) which has a rich literature. The RBDO perform design optimization in conjunction with reliability analysis by defining probabilistic constraints due to the presence of random variables. There are two major approaches for RBDO in the literature: the Reliability Index Approach (RIA), which directly presents the probabilistic constraint in the optimization; and the Performance Measure Approach (PMA), which constructs target performance function(s) by an inverse reliability analysis [16]. The two approaches are usually implemented in conjunction with a first-order reliability method (FORM), which is an approximation method of reliability analysis. There are also some variations of these two approaches, for example, Royset *et al.* [17, 18, 19] proposed decoupled RBDO formulations that use a more thorough inverse reliability analysis than the traditional FORM-based PMA and allows for heuristic updates of probability approximation.

Direct implementation of RIA or PMA results in a double loop optimization scheme since the reliability analysis or inverse reliability analysis requires an iterative process to find the most likely failure point or the most probable point (MPP) [16]. In order to reduce the computational cost, single loop algorithms [20, 21, 22, 23] have been developed, which employ the Karush-Kuhn-Tucker (KKT) conditions of the inner loop for a direct estimation of the FORM-based reliability analysis or inverse reliability analysis. Some authors have implemented these methods to solve RBTO problems. For example, Silva *et al.* [24] conducted a study comparing several selected RBDO algorithms including single loop PMA and double loop RIA. Nguyen *et al.*

[25] applied a single loop algorithm to SRBTO using a density based multi-resolution topology optimization (MTOP). Mogami *et al.* [26] employed a traditional double loop RIA to solve RBTO problems on ground structures. Other methods such as Monte Carlo simulation (MCS) based stochastic optimization [27] and equivalent perturbation based robust optimization [28] are also used to perform RBTO.

However, whether it is proper to directly apply RBDO methods to RBTO problems needs to be discussed. Unlike common RBDO problem, which usually involves several parameters to be optimized, RBTO has a large number of design variables, meaning that the solution space is of high dimension. For a gradient-based optimization, the accuracy of the sensitivity information may severely affect convergence. For DTO, there exists an analytical solution for the gradients of objective and constraint functions with respect to design variables. However, for RBTO, an analytical solution for the sensitivity of the probabilistic constraint has not been clearly addressed in the context of the RBDO, and a one-point first order approximation of the sensitivity is widely used. Although many researchers have successfully applied RBDO algorithms to some RBTO problems, it is observed that those algorithms may not work for all problems. This research adopts RIA for RBTO with a new method that provides more accurate sensitivity than the FORM-based approximation which, in addition, improves the accuracy of the reliability analysis involved in the optimization.

1.2 Thesis Organization

This thesis is organized as follows. Chapter 2 gives a background knowledge about the ground structure approach. Chapter 3 reviews several popular reliability methods, and revisits the RIA and PMA by analyzing the KKT optimality conditions. An analytical expression for the sensitivity of failure probability is also derived. In Chapter 4, the complete formulation of the new algorithm is addressed. The new technique for sensitivity calculation is proposed and its auxiliary benefits on improving reliability analysis is stated. The optimizer used is also discussed. Then in Chapter 5, the new algorithm is compared with DTO and a FORM-based algorithm via several numerical examples. Finally, the conclusions are summarized in Chapter 6.

CHAPTER 2

GROUND STRUCTURE APPROACH

Configuration optimization of trusses and frames has been studied since 1900's. The first work in the truss layout optimization was developed by Michell [29] in 1904. He derived several important analytical solutions of optimal layout of structures. Nowadays, thanks to the dramatic progress of computer technology, the optimization problem is performed using efficient numerical methods. Among many approaches for truss layout optimization, the ground structure approach is one of the most popular approaches. Admittedly, there are some unsolved issues with ground structure approach, such as instability at nodes and intersection of members, but as intended to provide conceptual designs, the approach is still an attractive choice.

The ground structure is basically a dense truss structure obtained by interconnecting fixed node points. Although there is no rule for the placement of nodes, the most popular choice is to place them on an orthogonal grid. Fig. 2.1 shows different levels of a ground structure on a 4×4 orthogonal base grid. As we can see in Fig. 2.1d, a full level ground structure connects every pair of nodes. For more detailed information about the connectivity levels of ground structure, we refer to [2, 11, 12]. Overlapping members need to be removed to avoid numerical instability. In general, the more members in the ground structure, the larger solution space (for the topology) we have.

2.1 Nested Formulation

The nested formulation of the ground structure approach is used in this research. Another approach is called simultaneous formulation. The difference between the two formulations is how the equilibrium equation is handled in the optimization [15]. The simultaneous formulation is described as follows:

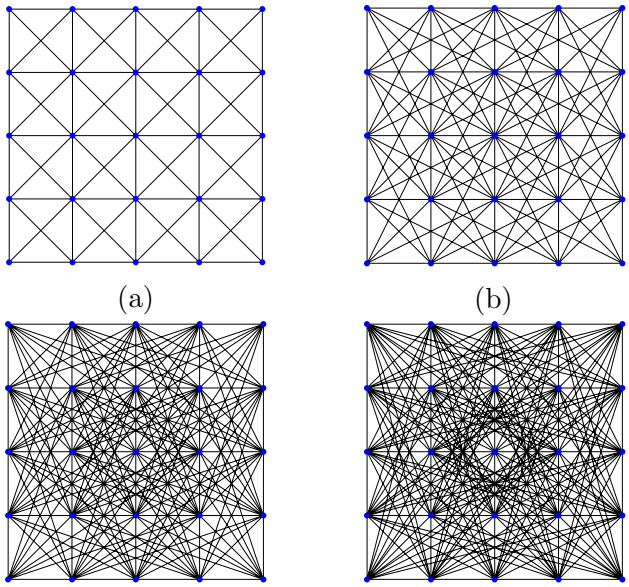

Figure 2.1: The four levels of the ground structure on a 4×4 grid. (a)Level 1: 72 non-overlapping members. (b)Level 2: 120 non-overlapping members. (c)Level 3: 176 non-overlapping members. (d)Level 4: 200 non-overlapping members.

$$\begin{aligned} \min_{\mathbf{x},\mathbf{d}} \quad & V = \boldsymbol{\rho}^{\mathrm{T}}\mathbf{b} \\ s.t. \quad & \mathbf{K}(\mathbf{x})\mathbf{d} = \mathbf{F} \\ & C(\mathbf{d}) - C^{max} \leqslant 0 \\ & \mathbf{x}_{min} \leqslant \mathbf{x} \leqslant \mathbf{x}_{max} \end{aligned} \tag{2.1}$$

where $\mathbf{b}$ is the volume vector of elements which is defined as product of element length and element area; $\boldsymbol{\rho}$ is a vector of material density which becomes a vector of 1's, if V represents the volume of the structure. $\mathbf{K}(\mathbf{x})\mathbf{d} = \mathbf{F}$ is the equation for equilibrium and compatibility of structure where $\mathbf{K}$ is the stiffness matrix, $\mathbf{d}$ is the nodal displacement vector and $\mathbf{F}$ is the load vector. $\mathbf{x}_{min}$ and $\mathbf{x}_{max}$ are the lower and upper bounds for design variables (i.e. member areas). The quantity C is defined as $C(\mathbf{d}) = \mathbf{l}^{\mathrm{T}}\mathbf{d}$, which is a linear combination of nodal displacement. In this research we take $\mathbf{l} = \mathbf{F}$, thus C becomes the total compliance of the structure. We know that compliance is the inner product of the external force vector and the nodal displacement

vector, which physically means the work done by external forces. Essentially, a structure with smaller compliance under given loads has a larger stiffness. The compliance and volume is a popular pair utilized in structural optimization, of which another common version is taking the compliance as the objective and volume as a constraint.

The main difference between simultaneous formulation and nested formulation is that the later one regards the compliance of structure under equilibrium as an implicit function of design variables. This results in the following optimization formulation:

$$\begin{aligned} \min_{\mathbf{x}} \quad & V = \boldsymbol{\rho}^{\mathrm{T}}\mathbf{b} \\ s.t. \quad & C(\mathbf{x}) - C^{max} \leqslant 0 \\ & \mathbf{x}_{min} \leqslant \mathbf{x} \leqslant \mathbf{x}_{max} \end{aligned} \tag{2.2}$$

where $C(\mathbf{x}) = \mathbf{F}^{\mathrm{T}}\mathbf{d}(\mathbf{x}) = \mathbf{F}^{\mathrm{T}}\mathbf{K}^{-1}(\mathbf{x})\mathbf{F}$, which indicates that we have to solve the linear system $\mathbf{d} = \mathbf{K}^{-1}(\mathbf{x})\mathbf{F}$ every time the compliance C is evaluated.

By comparing the two formulations, we can find that the nested formulation involves less design variables than the simultaneous formulation which has the nodal displacement as additional design variables. Nested formulation also eliminates a set of equality constraints in the optimization. Typically, for a DTO problem, the nested formulation leads to a convex programming problem with unique global optimum. Although this property is not preserved as we convert the problem into a probability constrained optimization, the nested formulation requires less computational cost since a linear system can be solved efficiently by many well developed numerical solvers.

The obtained optimal design will not remove any potential bars. To get the optimal topology, a typical approach is to apply a cutoff strategy: members with cross-sectional areas $x_i < \eta x_{max}$ will be ignored in the output topology, where η is an artificial parameter to control how much information is wanted. This strategy may present results with unbalanced nodes and unconnected elements, but mostly the topology will be clearly implied and serves well for purpose of conceptual design. However, this is still a field that can be improved for ground structure approach and will be considered in future

researches.

2.2 Sensitivity Analysis of Compliance

To perform a gradient-based optimization, the sensitivity is necessary. The derivatives of the volume is rather simple to derive since it is a linear function. The sensitivity of compliance, however, requires some efforts to obtain. Attributing to the effort researchers have done, the derivation of sensitivity of compliance can be found in many literatures [2, 15, 30]. There are two different methods to obtain the sensitivity, namely the direct differentiation method and the adjoint variable method. For compliance, both methods yield a same result. We will briefly summarize the process by the direct differentiation method since it is more straightforward than the other method.

We consider $C(\mathbf{x}) = \mathbf{F}^{\mathrm{T}}\mathbf{d}(\mathbf{x})$. Taking derivative with respect to x_j, since in this research $\mathbf{F}$ is not a function of $\mathbf{x}$, the derivative can be written as:

$$\frac{\partial C(\mathbf{x})}{\partial x_j} = \mathbf{F}^{\mathrm{T}}\frac{\partial \mathbf{d}(\mathbf{x})}{\partial x_j} \tag{2.3}$$

The derivative of the equilibrium equation with respect to x_j is given by:

$$\frac{\partial \mathbf{K}(\mathbf{x})}{\partial x_j}\mathbf{d} + \mathbf{K}(\mathbf{x})\frac{\partial \mathbf{d}}{\partial x_j} = \frac{\partial \mathbf{F}}{\partial x_j} = \mathbf{0} \tag{2.4}$$

Rearranging terms of Eq. (2.4), we obtain:

$$\begin{aligned}\frac{\partial \mathbf{d}(\mathbf{x})}{\partial x_j} &= -\mathbf{K}^{-1}\frac{\partial \mathbf{K}}{\partial x_j}\mathbf{d} \\ &= -\mathbf{K}^{-1}\frac{\partial(\sum_{j=1}^{m} x_j\mathbf{K}_j^0)}{\partial x_j}\mathbf{d} \\ &= -\mathbf{K}^{-1}\mathbf{K}_j^0\mathbf{d}\end{aligned} \tag{2.5}$$

where $\mathbf{K}_j^0$ is the element stiffness matrix of the j^{th} element in global coordinates of degrees of freedom divided by the member area x_j, which is called constant element stiffness matrix [15]; and m is the number of elements (i.e. number of design variables). Substituting Eq. (2.5) to Eq. (2.3), and considering the symmetry of the stiffness matrix $\mathbf{K}$, we obtain:

$$\frac{\partial C}{\partial x_j} = -\mathbf{d}^{\mathrm{T}} \mathbf{K}_j^0 \mathbf{d} \tag{2.6}$$

Eq. (2.6) is not very costly to compute since $\mathbf{K}_j^0$ is a sparse matrix with only 16 non-zero entries at most, but it requires to be evaluated component-wise of $\mathbf{x}$.

CHAPTER 3

RELIABILITY-BASED DESIGN OPTIMIZATION

3.1 Reliability Methods

In this section, we will briefly review several most popular reliability methods, namely the first-order reliability method (FORM), the second-order reliability method (SORM) and Monte Carlo simulation (MCS). We will not discuss much details, thus for further interest, we refer to [31, 32, 33]. The methods of reliability theory are concerned with estimating the failure probability, P_f, of engineering system. In the context of structural reliability, reliability index, β, is a common measure of reliability which is defined as $\beta = \Phi^{-1}(1 - P_f)$, where $\Phi(\cdot)$ is the cumulative distribution function (CDF) of a standard normal distribution and $\Phi^{-1}(\cdot)$ is its inverse operation.

Consider a set of random variables $\mathbf{v}$ with a joint probability density function (PDF), $f_{\mathbf{v}}(\mathbf{v})$. A function $g(\mathbf{v})$, called a limit state function, is defined to determine the Boolean status of either safe or fail. By convention, a realization of $\mathbf{v}$ that makes $g(\mathbf{v}) \leqslant 0$ is a failure event. And the surface described by $g(\mathbf{v}) = 0$ is called limit state surface which delimits the failure domain and safe domain in the random space. Mathematical expression for P_f leads to an integration:

$$P_f = \int_{g(\mathbf{v})\leqslant 0} f_{\mathbf{v}}(\mathbf{v})\mathrm{d}\mathbf{v} \tag{3.1}$$

Since the joint distribution of original random variables are usually difficult ot deal with. To perform a reliability analysis, a common initiation is to perform a probability preserving transformation $\mathbf{u} = T(\mathbf{v})$, where $\mathbf{u}$ is a vector of independent standard normal random variables. This will transform Eq. (3.1) into:

$$P_f = \int_{G(\mathbf{u})\leqslant 0} \varphi_n(\mathbf{u}) \mathrm{d}\mathbf{u} \tag{3.2}$$

where $\varphi_n(\cdot)$ is the multi-variate standard normal PDF with uncorrelated components and $G(\mathbf{u}) = g(T^{-1}(\mathbf{u}))$. However, the integral in Eq. (3.2) is not tractable to compute, especially in multidimensional random space. Hence, numerical methods are developed to approximate P_f.

One approach is by taking samples and collecting the discrete data to estimate P_f. Since a set of independent standard normal distribution can be generated using well-developed numerical processes, a MCS is often performed by first generating a large number of realizations of $\mathbf{u}$ and transforming them back to the original random space of $\mathbf{v}$. The probability of failure is then approximated as:

$$P_f \approx \frac{1}{N} \sum_{i=1}^{N} I(\mathbf{v}) \tag{3.3}$$

where N is the number of samples and $I(\mathbf{v})$ is an indicator function:

$$I(\mathbf{v}) = \begin{cases} 1 & \text{if } g(\mathbf{v}) \leqslant 0 \\ 0 & \text{if } g(\mathbf{v}) > 0 \end{cases} \tag{3.4}$$

There are many variations of MCS but we will limit our discussion on the basic ideas.

The standard normal space of transformed random variables $\mathbf{u}$ is rotational symmetric and the value of $\varphi_n(\mathbf{u})$ decays exponentially as moving away from the origin. Based on these properties, the FORM takes a linear expansion of the limit state surface at the point of maximum probability density which is called the most likely failure point (as shown in Fig. 3.1). This point is also named a design point or, the most central point. The point is conventionally denoted as $\mathbf{u}^*$, and it is defined as follows:

$$\mathbf{u}^* = \underset{\mathbf{u}}{\operatorname{argmin}} \{ \|\mathbf{u}\| \mid G(\mathbf{u}) = 0 \} \tag{3.5}$$

By definition, the most likely failure point is the closet point to the origin on the limit state surface. The linear expansion at this point yields an approximated failure probability as

$$P_f \approx 1 - \Phi(\|\mathbf{u}^*\|) = \Phi(-\|\mathbf{u}^*\|) \tag{3.6}$$

which only requires a little computational cost. If the reliability index measured by FORM is denoted as β_1, it is straightforward to obtain that $\beta_1 = \|\mathbf{u}^*\|$. The effort to find $\mathbf{u}^*$ is mathematically an optimization problem with equality constraint. Researchers have developed algorithm particularly for this kind of problem, which is called HL-RF algorithm, named after Hasofer, Lind, Rackwitz, and Fiessler [34]. An improved version of the HL-RF algorithm proposed by Zhang and Der Kiureghian [35] employs line-searching and damping parameter to make the original version more robust. Essentially, the improved HL-RF algorithm is categorized to the family of Steepest-Descent algorithms.

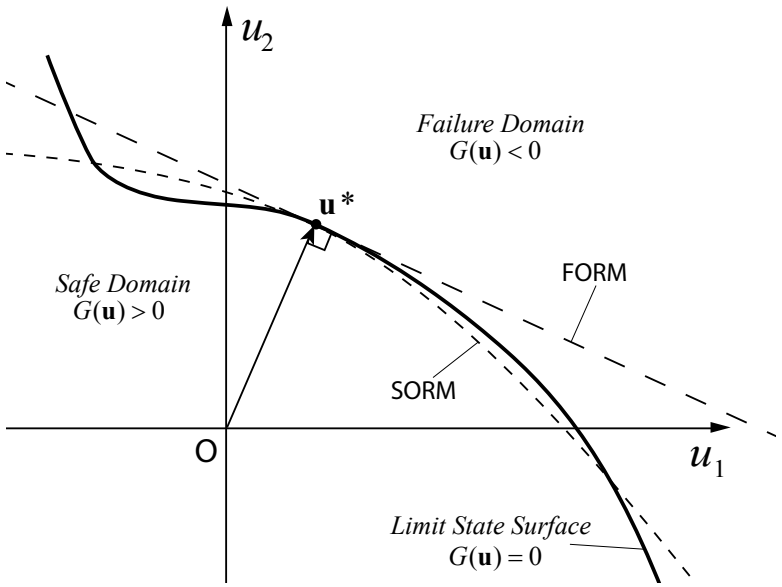

Figure 3.1: Illustration of FORM and SORM.

In order to improve the accuracy, researchers further considered using a second-order quadratic expansion of the limit state surface. The expansion is also taking at the most likely failure point since the region near the most likely failure point is of the most importance as it has relatively high probability density. The second order expansion requires information about the Hessian of limit state function. The Hessian is the matrix contains second order derivatives of a function which is usually expensive to compute. In addition, an eigenvalue analysis of the Hessian needs to be performed in order to

obtain the principle curvatures of the limit state surface, since the solution for probability integral with quadratic limit state function is written in terms of principle curvatures. Different methods have been proposed to compute the principle curvature and many times approximation is used. Moreover, the exact result for probability integral with quadratic limit state function proposed by Tvedt still requires integration [32]. The current known SORM is essentially based on an expression proposed by Breitung [36]. This simple and famous result is obtained by an asymptotic analysis as:

$$P_f \approx \Phi(-\beta_1) \prod_{i=1}^{n-1} (1 - \beta_1 \kappa_i)^{-1/2} \tag{3.7}$$

where κ_i's are the principle curvatures of the limit state surface at $\mathbf{u}^*$ and n is the number of transformed random variables. Intuitively, the result can be regarded as an update of FORM by a curvature correction term. However, this expression is only valid for $\beta_1 \geqslant 1$ and $\beta_1 \kappa_i \leqslant 1$ for all i [32].

For practical applications, FORM often tends to be sufficiently accurate, and it is the most popular technique for reliability assessment that is required in RBDO algorithms.

3.2 A Review of RBDO Approaches

In this section, previous approaches of RBDO will be revisited via a check of KKT optimality conditions. Consider a generic formulation of RBDO problems with one reliability component:

$$\begin{aligned} &\min_{\mathbf{x}} f(\mathbf{x}) \\ s.t. \quad &P_f = \int_{G(\mathbf{x},\mathbf{u})<0} \varphi_n(\mathbf{u}) \mathrm{d}\mathbf{u} \leqslant P_f^t \\ &\mathbf{h}(\mathbf{x}) \leqslant \mathbf{0} \end{aligned} \tag{3.8}$$

where P_f^t is the target failure probability; $\mathbf{x}$ is the vector of design variables; $\mathbf{u}$ is the vector of transformed random variables; $f(\mathbf{x})$ is the objective function; $G(\mathbf{x}, \mathbf{u})$ is the limit state function that defines failure event; and $\mathbf{h}(\mathbf{x})$ is a set of deterministic constraints such as lower and upper bounds of $\mathbf{x}$.

Theoretically, the KKT optimality conditions of the mathematical model of RBDO (Eq. 3.8) would become:

1. Stationary condition: $\nabla_{\mathbf{x}} f + \lambda \nabla_{\mathbf{x}} P_f + \sum \gamma_i \nabla_{\mathbf{x}} h_i = 0$
2. Primal feasibility: $P_f - P_f^t \leqslant 0$, $h_i \leqslant 0 \; \forall i$
3. Dual feasibility: $\lambda \geqslant 0$, $\gamma_i \geqslant 0 \; \forall i$
4. Complementary slackness: $\lambda(P_f - P_f^t) = 0$, $\gamma_i h_i = 0 \; \forall i$

where λ and γ_i's are Lagrange multipliers. The KKT conditions are necessary for a solution to be optimal. In RBDO, due to the presence of probabilistic constraint, the stationary condition and primal feasibility are only approximately satisfied at the optimum. Different RBDO algorithms have different approximations about the KKT conditions and may differ with the process to achieve a solution. We will show that RIA and PMA share the same approximations about the KKT conditions, in particular $\nabla_{\mathbf{x}} P_f$ and P_f, and RBDO algorithms based on first order expansion of the limit state function, may not work for RBTO.

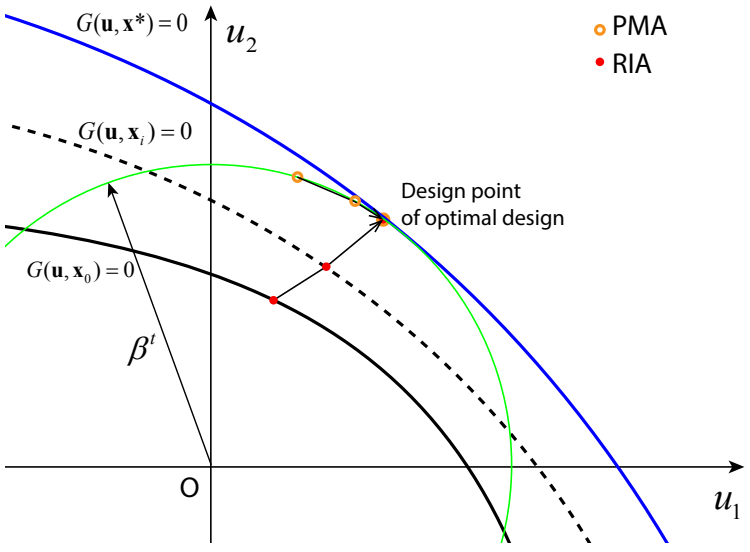

Figure 3.2: Trajectory of the optimization process of RIA and PMA in the standard normal random space.

In the RIA formulation, the reliability constraints are considered directly. The sensitivity of failure probability with respect to design variables is used

to get the search direction in topology optimization. An analytical expression for the derivative $\nabla_{\mathbf{x}}\beta$ is derived by Hohenbichler and Rackwitz [37] under assumption of an affine limit state function.

$$\nabla_{\mathbf{x}}\beta = \frac{1}{\|\nabla_{\mathbf{u}}G^*\|}\nabla_{\mathbf{x}}G^* \tag{3.9}$$

where G^* denotes $G(\mathbf{x}, \mathbf{u}^*)$, which is the limit state function evaluated at the design point $\mathbf{u}^*$ with current design $\mathbf{x}$ when it is evaluated. Since $P_f = 1 - \Phi(\beta)$, we have $\mathrm{d}P_f/\mathrm{d}\beta = -\varphi(\beta)$. By applying the chain rule, we obtain:

$$\nabla_{\mathbf{x}}P_f = -\frac{\varphi(\beta)}{\|\nabla_{\mathbf{u}}G^*\|}\nabla_{\mathbf{x}}G^* \tag{3.10}$$

The KKT stationary condition of RIA is then given by:

$$\nabla_{\mathbf{x}}f + \lambda^{RIA}\left[-\frac{\varphi(\beta)}{\|\nabla_{\mathbf{u}}G^*\|}\nabla_{\mathbf{x}}G^*\right] + \sum \gamma_i \nabla_{\mathbf{x}}h_i = 0 \tag{3.11}$$

As stated before, Eq. (3.9) and (3.10) are derived based on the assumption that the limit state function is affine. For nonlinear limit state functions, the expressions can be regarded as the sensitivity of the reliability index obtained by FORM (i.e. β_1). Thus, in the rest of this thesis, Eqs. (3.9) and (3.10) will be stated as FORM-based sensitivity approximation. In general, differentiation of an approximate expression would enlarge the error. Therefore, some times even though the FORM provides a good approximation of the P_f, the sensitivity $\nabla_{\mathbf{x}}P_f$ calculated by FORM-based approximation could have a large error.

The PMA formulation applies inverse FORM reliability analysis. The approach defines a target performance function $G^t(\mathbf{x}) = G(\mathbf{x}, \mathbf{u}^t)$ and incorporates it as it is a deterministic constraint of topology optimization, where $\mathbf{u}^t$ is an estimation of the design point of the optimal design which is also called the most probable point (MPP) and is updated at each iteration as

$$\mathbf{u}^t = \underset{\mathbf{u}}{\operatorname{argmin}}\{G(\mathbf{x}, \mathbf{u}) \mid \|\mathbf{u}\| = \beta^t = \Phi^{-1}(1 - P_f^t)\} \tag{3.12}$$

Usually approximated $\mathbf{u}^t$ is used to reduce computational cost. The advantage of PMA is that it is not very sensitive to the accuracy of $\mathbf{u}^t$, thus single loop algorithms, which involve a coarse approximation of $\mathbf{u}^t$, are usually developed based on PMA. However, when the optimum is achieved and

the probabilistic constraint become active, $\mathbf{u}^t$ converges to the design point of the final design [16]. The KKT stationary condition of the PMA becomes:

$$\nabla_{\mathbf{x}} f + \lambda^{PMA}(-\nabla_{\mathbf{x}} G^*) + \sum \gamma_i \nabla_{\mathbf{x}} h_i = 0 \tag{3.13}$$

Equation (3.11) and (3.13) are the same except the second term that has a different coefficient. If the probabilistic constraint is active and the design point is unique, the two approaches will yield $\lambda^{PMA} = \frac{\varphi(\beta)}{\|\nabla_{\mathbf{u}} G^*\|}\lambda^{RIA}$, thus the KKT conditions become identical. Hence, although PMA tends to be more robust than RIA, it does not improve the result of the optimization since it is mathematically equivalent to RIA when the problem is well posed. If we look at the iteration process, PMA and RIA have different paths to achieve the same design point of the same "optimal" design. The trajectories of RIA and PMA in the random space are illustrated in Fig. 3.2, where $\mathbf{x}^*$ refers to the "optimal" design, $\mathbf{x}_0$ is the initial design, and $\mathbf{x}_i$ represent one intermediate design of the optimization process.

Many algorithms which are developed based on RIA and PMA incorporate SORM, MCS or other reliability methods to improve the approximation of the primal feasibility condition (i.e. P_f) [19, 25], but little attention has been paid to the accuracy of the stationary condition which is instead more influential to the optimal topology than the feasibility condition. Furthermore, the error in sensitivity is cumulative since it determines the search direction at each iteration of gradient-based optimization scheme. Since the obtained stationary condition is approximated based on an one-point linear expansion of the limit state surface, for problems with a nonlinear limit state surface like RBTO, the validity of using FORM-based algorithms need to be reconsidered.

3.3 Gradient of Probability Function

In order to examine the influence of the error introduced by the approximation of $\nabla_{\mathbf{x}} P_f$ in FORM-based approaches, an analytical solution of $\nabla_{\mathbf{x}} P_f$ for general limit state functions is needed. In the derivation, we will only assume that the limit state function is smooth and continuous.

Based on the assumption, for each point on the limit state surface, if we

take a perturbation $\delta\mathbf{x}$ on the design variables, it would move to a new location in the random variable space. If the movement is denoted as $\delta\mathbf{u}$, the following equation has to be satisfied

$$\delta G(\mathbf{u},\mathbf{x}) = \nabla_{\mathbf{x}} G(\mathbf{u},\mathbf{x})\delta\mathbf{x} + \nabla_{\mathbf{u}} G(\mathbf{u},\mathbf{x})\delta\mathbf{u} = 0 \tag{3.14}$$

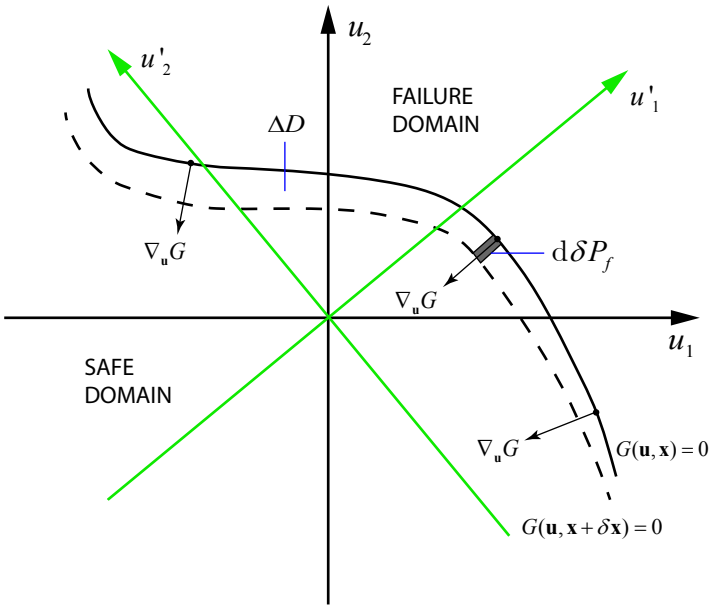

Figure 3.3: Geometric representation of general continuous limit state surface.

The limit state surface in the $\mathbf{u}$-space can be regarded as a level set of the surface $G(\mathbf{u},\mathbf{x}) = 0$ in the hybrid space of random variables $\mathbf{u}$ and design variables $\mathbf{x}$ at a certain level of $\mathbf{x}$. The coordinates $\mathbf{x}$ are orthogonal to $\mathbf{u}$ since the random variables are independent from the design variables. Hence, the small change $\delta\mathbf{u}$, which is due to the perturbation $\delta\mathbf{x}$, will along the same direction of $\nabla_{\mathbf{u}} G(\mathbf{u},\mathbf{x})$. We rotate the coordinate system of the $\mathbf{u}$-space such that the axis $\mathbf{e}'_1$ is in the opposite direction of $\nabla_{\mathbf{u}} G(\mathbf{u},\mathbf{x})$. Denote the new coordinates as $\mathbf{u}' = \mathbf{Q}\mathbf{u} = [u'_1, \hat{\mathbf{u}}']^{\mathrm{T}}$, where the rotational operator $\mathbf{Q}$ is a function of $\mathbf{u}$ and $\mathbf{x}$. Notice that $\mathbf{Q}$ is not the same for different points on limit state surface. Then Eq. (3.14) can be rewritten in the form as:

$$\delta G(\mathbf{u},\mathbf{x}) = \nabla_{\mathbf{x}} G(\mathbf{u},\mathbf{x})\delta\mathbf{x} + \|\nabla_{\mathbf{u}} G(\mathbf{u},\mathbf{x})\|\delta u'_1 = 0 \tag{3.15}$$

The change of failure probability due to a perturbation of $\mathbf{x}$ is the integration of probability density function over the change of the failure domain. The

change of failure domain is denoted as ΔD, which is the region between the dashed curve and solid curve in Fig. 3.3. Thus we can obtain:

$$\delta P_f = \int_{G(\mathbf{u},\mathbf{x}+\delta\mathbf{x})\leqslant 0} \varphi(\mathbf{u})\mathrm{d}\mathbf{u} - \int_{G(\mathbf{u},\mathbf{x})\leqslant 0} \varphi(\mathbf{u})\mathrm{d}\mathbf{u} = \int_{\Delta D} \varphi(\mathbf{u})\mathrm{d}\mathbf{u} \tag{3.16}$$

Taking a small piece of the ΔD and calculating the volume under the probability density function, we obtain:

$$\mathrm{d}\delta P_f = \varphi_n(\mathbf{u}')\delta u_1' \delta\hat{\mathbf{u}}' \tag{3.17}$$

where $\delta\hat{\mathbf{u}}' = \delta u_2'\delta u_3'...\delta u_n'$ and n is the number of random variables. Substituting (3.15) into (3.17), we obtain

$$\mathrm{d}\delta P_f = -\varphi_n(\mathbf{u}')\frac{\nabla_{\mathbf{x}} G\delta\mathbf{x}}{\|\nabla_{\mathbf{u}} G\|}\delta\hat{\mathbf{u}}' \tag{3.18}$$

Taking the limit $\delta\mathbf{u} \to 0$ and integrating $\mathrm{d}\delta P_f$ over the limit state surface, an integral expression for the change of failure probability is obtained:

$$\delta P_f = \int_{S'} \mathrm{d}\delta P_f = \int_{S'} -\varphi_n(\mathbf{u}')\frac{\nabla_{\mathbf{x}} G\delta\mathbf{x}}{\|\nabla_{\mathbf{u}} G\|}\mathrm{d}\hat{\mathbf{u}}' \tag{3.19}$$

where S and S' are the limit state surface in original coordinates and rotated coordinates. Rearranging the terms, we can get the sensitivity of the failure probability with respect to design variables as:

$$\frac{\partial P_f}{\partial \mathbf{x}} = \frac{\delta P_f}{\delta \mathbf{x}} = \int_{S'} -\varphi_n(\mathbf{u}')\frac{\nabla_{\mathbf{x}} G}{\|\nabla_{\mathbf{u}} g\|}\mathrm{d}\hat{\mathbf{u}}' = \int_{S'} -\frac{\varphi_n(\mathbf{u}')}{\|\nabla_{\mathbf{u}} g\|}\nabla_{\mathbf{x}} G\mathrm{d}S' \tag{3.20}$$

Although $\mathbf{Q}$ is not a constant operator, since rotational matrix is orthogonal, the determinant of $\mathbf{Q}$ always has the value 1. Hence, $\mathrm{d}S' = (\det\mathbf{Q})\mathrm{d}S = \mathrm{d}S$. Also since the standard normal space is rotational symmetric, $\varphi_n(\mathbf{u}') = \varphi_n(\mathbf{u})$. Eq. (3.20) can be rewritten in the original coordinate as

$$\frac{\partial P_f}{\partial \mathbf{x}} = -\int_S \frac{\varphi_n(\mathbf{u})}{\|\nabla_{\mathbf{u}} G\|}\nabla_{\mathbf{x}} G\mathrm{d}S \tag{3.21}$$

A different version of Eq. (3.21) has been proposed by Royset and Polak [27] that is derived inversely from discrete form of failure probability. Also a more complete expression is found in the paper by Uryasev [38] published in

1994 where the probability distributions of $\mathbf{u}$ are considered also a function of $\mathbf{x}$. The expression for the gradient of failure probability with respect to design variable is a surface integral over the limit state surface. Thus for the FORM-based approximation, which is calculated only at the design point, the error can be very large since a lot of information is missing. For example, if the design have an impact on the curvature of the limit state surface, the approximated sensitivity which is based on linear expansion at one point on limit state surface would never capture this kind of influence. This will be illustrated in the first numerical example. In spite of the fact that the influence of this error differs for different problems because some problems are sensitive to search direction while some are not, examples reveal that the error in sensitivity computation can exceed the tolerance of RBTO problems. In the case of limit state functions with multiple design points, which is not very rare in RBTO problems, it is reported that FORM-based algorithms have convergence issues [24].

In the following, we will show that when applying to affine limit state function, Eq. (3.21) will be the same with Eq. (3.10). Consider an affine limit state function:

$$G(\mathbf{u}, \mathbf{x}) = \mathbf{a}(\mathbf{x})^{\mathrm{T}}\mathbf{u} + b(\mathbf{x}) \tag{3.22}$$

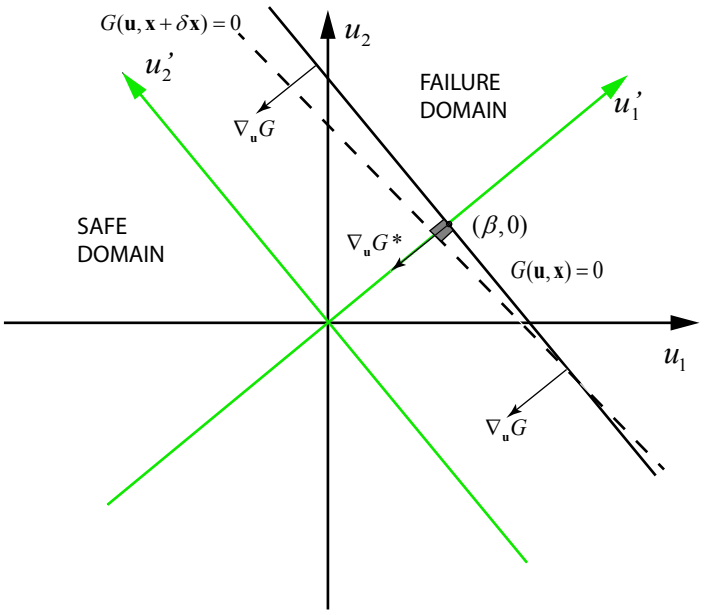

Figure 3.4: Geometric representation of affine limit state surface.

And we have:

$$\nabla_{\mathbf{x}} G = [\nabla \mathbf{a}]\mathbf{u} + \nabla b \tag{3.23}$$

where $\mathbf{a}(\mathbf{x})$ is a vector function of $\mathbf{x}$ and $b(\mathbf{x})$ is a scalar function of $\mathbf{x}$. Because the function is affine in $\mathbf{u}$, $\nabla_{\mathbf{u}} G$ remains a constant vector for a given design $\mathbf{x}$. Thus by the definition of the operator $\mathbf{Q}$, it will also remain unchanged for each point on the limit state surface. Denoting $\mathbf{u}^*$ as the design point, we now have

$$\mathbf{u}'^* = \begin{bmatrix} \beta \\ \mathbf{0} \end{bmatrix} = \mathbf{Q}\mathbf{u}^* \tag{3.24}$$

where $\beta = \|\mathbf{u}^*\|$, which is the reliability index. Other points on the limit state surface can be expressed as:

$$\mathbf{u}' = \begin{bmatrix} \beta \\ \hat{\mathbf{u}}' \end{bmatrix} = \mathbf{Q}\mathbf{u} \tag{3.25}$$

where the first component is the same with the design point and the other components are denoted as $\hat{\mathbf{u}}'$. Due to the fact that $\varphi_n(\mathbf{u}) = \varphi_n(\mathbf{u}') = \varphi(\beta)\varphi_{n-1}(\hat{\mathbf{u}}')$, Eq. (3.21) can be rewritten in the following way:

$$\begin{aligned} \nabla_{\mathbf{x}} P_f &= -\int_{S'} \frac{\varphi(\beta)\varphi_{n-1}(\hat{\mathbf{u}}')}{\|\nabla_{\mathbf{u}} G\|} \nabla_{\mathbf{x}} G \mathrm{d}S' \\ &= -\frac{\varphi(\beta)}{\|\nabla_{\mathbf{u}} G^*\|} \int_{S'} \varphi_{n-1}(\hat{\mathbf{u}}') \nabla_{\mathbf{x}} G \mathrm{d}S' \end{aligned} \tag{3.26}$$

Substituting Eq. (3.23) and Eq. (3.25) in Eq. (3.26), we have:

$$\begin{aligned} \nabla_{\mathbf{x}} P_f &= -\frac{\varphi(\beta)}{\|\nabla_{\mathbf{u}} G^*\|} \int_{S'} \varphi_{n-1}(\hat{\mathbf{u}}') \left([\nabla \mathbf{a}]\mathbf{Q}^{-1} \begin{bmatrix} \beta \\ \hat{\mathbf{u}}' \end{bmatrix} + \nabla b \right) \mathrm{d}S' \\ &= -\frac{\varphi(\beta)}{\|\nabla_{\mathbf{u}} G^*\|} \int_{S'} \varphi_{n-1}(\hat{\mathbf{u}}') \left[[\nabla \mathbf{a}]\mathbf{Q}^{-1} \left(\begin{bmatrix} \beta \\ \mathbf{0} \end{bmatrix} + \begin{bmatrix} 0 \\ \hat{\mathbf{u}}' \end{bmatrix} \right) + \nabla b \right] \mathrm{d}S' \end{aligned} \tag{3.27}$$

Realizing that $\varphi_{n-1}(\hat{\mathbf{u}}')$ is an even function of $\hat{\mathbf{u}}'$ and $[\nabla \mathbf{a}]\mathbf{Q}^{-1} \begin{bmatrix} 0 \\ \hat{\mathbf{u}}' \end{bmatrix}$ is an odd

function, the integration yields:

$$\nabla_{\mathbf{x}} P_f = -\frac{\varphi(\beta)}{\|\nabla_{\mathbf{u}} G^*\|} \int_{S'} \varphi_{n-1}(\hat{\mathbf{u}}') \left([\nabla \mathbf{a}] \mathbf{T}^{-1} \begin{bmatrix} \beta \\ \mathbf{0} \end{bmatrix} + \nabla b \right) \mathrm{d}S' \tag{3.28}$$

Substituting Eq. (3.23) and (3.24) in Eq. (3.28), since $\int_{S'} \varphi_{n-1}(\hat{\mathbf{u}}')\mathrm{d}S' = 1$, we can obtain:

$$\begin{aligned} \nabla_{\mathbf{x}} P_f &= -\frac{\varphi(\beta)}{\|\nabla_{\mathbf{u}} G^*\|} \int_{S'} \varphi_{n-1}(\hat{\mathbf{u}}') \nabla_{\mathbf{x}} G^* \mathrm{d}S' \\ &= -\frac{\varphi(\beta)}{\|\nabla_{\mathbf{u}} G^*\|} \nabla_{\mathbf{x}} G^* \int_{S'} \varphi_{n-1}(\hat{\mathbf{u}}') \mathrm{d}S' \\ &= -\frac{\varphi(\beta)}{\|\nabla_{\mathbf{u}} G^*\|} \nabla_{\mathbf{x}} G^* \end{aligned} \tag{3.29}$$

Finally Eq. (3.10) by Hohenbichler and Rackwitz [37] which is developed based on affine assumption of limits state function is recovered from the general integral form of derivative of failure probability.

CHAPTER 4

RELIABILITY-BASED TOPOLOGY OPTIMIZATION FORMULATION

Inherited from the nested formulation described in Chapter 2, the mathematical formulation of the RBTO problem considered in this thesis is stated as follows:

$$\begin{aligned} &\min_{\mathbf{x}} \quad V = \mathbf{1}^{\mathrm{T}}\mathbf{b} \\ s.t. \quad &P[C(\mathbf{x}) - C^{max} < 0] - P_f^t \leqslant 0 \\ &\mathbf{x}_{min} \leqslant \mathbf{x} \leqslant \mathbf{x}_{max} \end{aligned} \tag{4.1}$$

where $\mathbf{1}$ is a vector of 1's as mentioned in Chapter 2. The design variables $\mathbf{x}$ are member areas of the ground structure. The only difference between formulation (4.1) with (2.2) is that the deterministic constraint on the compliance becomes a probabilistic constraint due to the introduction of random variables. A small value $\epsilon = 10^{-4}$ is assigned to $\mathbf{x}_{min}$ in order to prevent singularity of the structural stiffness matrix $\mathbf{K}$.

Based on the formulation, the RBTO algorithm is developed in the manner of RIA, where we directly state the probability constraint in the optimization. Different from the traditional RIA, the sensitivity will be calculated using a new approximation. Details about the new approximation is addressed in Section 1 of this Chapter. Section 2 discusses the auxiliary benefit of this method on reliability assessment. Finally, the optimization algorithm is discussed in Section 3.

4.1 Segmental Multi-Point Linearization for Sensitivity Calculation

For most cases, the integral in Eq. (3.21) is not computationally tractable since it is a multi-dimensional surface integral. However, we can make approximation by taking multi-point linearization of the limit state surface. As the term $\frac{\varphi_n(\mathbf{u})}{\|\nabla_{\mathbf{u}} G\|}$ is just a scalar, the integral can be regarded as a weighted sum of $\nabla_{\mathbf{x}} G$ on the limit state surface. Inspired by numerical integration, instead of integrating over the curved surface, the proposed method takes a multi-point discrete representation of the integral. Eq. (3.10) can be regarded as a one-point discrete representation of Eq. (3.21). A discrete representation can be described in the following form:

$$\begin{aligned} \nabla_{\mathbf{x}} P_f &= -\int_S \frac{\varphi_n(\mathbf{u})}{\|\nabla_{\mathbf{u}} G\|} \nabla_{\mathbf{x}} G \mathrm{d}S \\ &\approx \sum_{j=1}^{p} W_j \nabla_{\mathbf{x}} G^j \end{aligned} \tag{4.2}$$

where W_j is the corresponding weight for $\nabla_{\mathbf{x}} G^j$ evaluated at point j and p is the number of discrete components $\nabla_{\mathbf{x}} G^j$. The approximation of $\nabla_{\mathbf{x}} P_f$ involves two main steps: (1) choose sample points; (2) calculate weight W_j based on a local linearization of limit state surface around sample points. Eq. (3.10) can be regarded as a special case where the only one sample point is chosen to be the design point and the weight is calculated to be $-\frac{\varphi(\beta)}{\|\nabla_{\mathbf{u}} G^*\|}$ by taking a tangent linearization of the limit state surface at the design point.

There are several guidelines for choosing the sample points. First, since Eq. (3.21) is a surface integral, the sample points should not be away from the surface. Second, the information should be collected from the region that is close to the origin of the **u**-space. The reason is that the value of $\varphi(\mathbf{u})$ only depends on the distance of the point to the origin in the standard normal space (i.e. $\|\mathbf{u}\|$) and decays very quickly as the distance increases. Additionally, the sample points should not be too close to each other in order to avoid repetitive information since based on our assumption there is no jumps in the function and $\nabla_{\mathbf{x}} G$ and $\nabla_{\mathbf{u}} G$ should vary smoothly. Based on these guidelines, we propose a simple scheme to determine the sample points systematically.

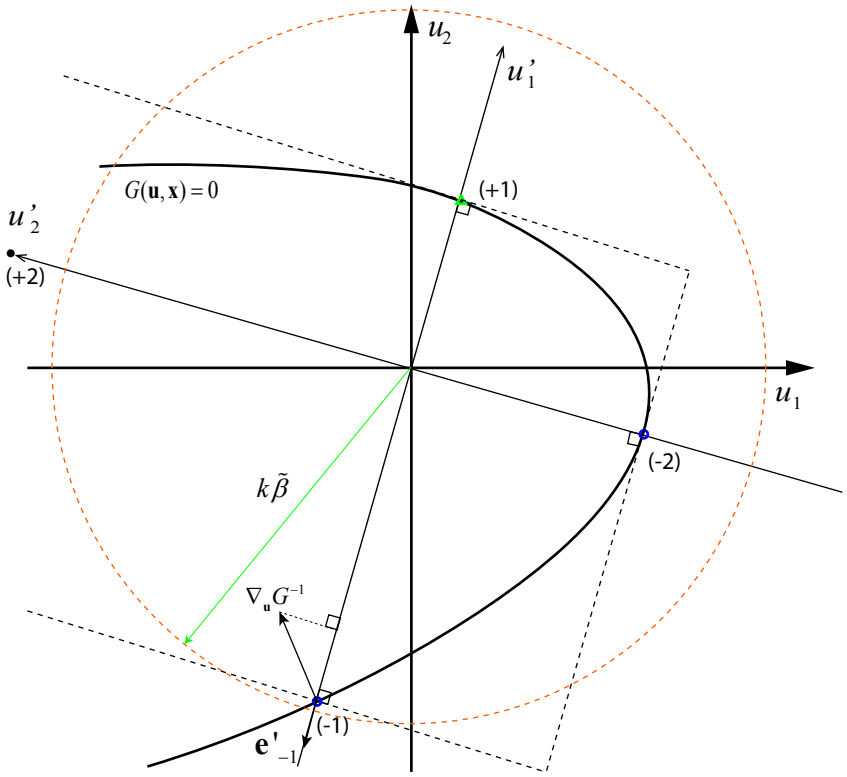

Figure 4.1: Graphical illustration of the proposed segmental multi-point linearization method (SML), where green triangle refers to the reference point, blue circles refer to sample point, $(\pm i)$ represent $\mathbf{u}^{(\pm i)}$.

The method is summarized as follows:

1. Select a reference point $\mathbf{u}^{(+1)}$;

2. Rotate the coordinates such that the reference point lies on the positive part of the first axis of the new coordinates;

3. Search for intersection points of the new axes and the limit state surface within radius $r = k\tilde{\beta}$ from the origin, where k is a user defined parameter and $\tilde{\beta}$ is the approximated reliability index of current design.

4. Finally the sample points are taken as the intersection points including the reference point.

The rotation of coordinates is achieved by a constant orthogonal transformation $\mathbf{R}$ such that $\mathbf{u}'^{(+1)} = \mathbf{R}\mathbf{u}^{(+1)} = [\|\mathbf{u}^{(+1)}\|, 0, \ldots, 0]^{\mathrm{T}}$. The rotational matrix $\mathbf{R}$ is easy to compute by replacing the first column of an identity matrix by $\mathbf{u}^{(+1)}/\|\mathbf{u}^{(+1)}\|$ and applying a QR factorization to the matrix, for

example, a Gram-Schmidt process. We denote the positive direction of the new axes i as $\mathbf{e}'_{+i}$ and the negative as $\mathbf{e}'_{-i}$. The computation of the intersection points can be done by solving the 1D nonlinear equation $G(\mathbf{x}, \alpha_i(\mathbf{e}'_i)) = 0$ for α_i and the solution is simply $\alpha_i \mathbf{e}'_i$. There are many well developed algorithms that are efficient and robust for solving 1D nonlinear equations such as the bisection method. If for one direction there is no intersection point inside the hypersphere with $r = k\tilde{\beta}$, we will assume that the intersection point is located at infinity (i.e. no intersection). For example, point $\mathbf{u}^{(+2)}$ in Fig. 4.1 is not a sample point and it is taken to be at the infinity of direction $\mathbf{e}'_{+2}$. The parameter k defines how large the search region is. Mostly, it should have a value between 2 and 5 in order to make sure that nonlinearity of the limit state surface is captured by the sample points that are too far from the origin. The reference point is the intersection of the limit state surface with the positive part of axis 1.

To determine the weights, first the limit state surface is linearized at the sample points such that it is approximated by several segments of hyperplanes. For example, we assume that the j^{th} sample point is on the positive direction of axis i and it is denoted as $\mathbf{u}^{(+i)}$. The hyperplane determined by $\mathbf{u}^{(+i)}$ must pass the sample point and be orthogonal to $\mathbf{e}_{+i}$. The gradient with respect to $\mathbf{u}$ of the affine function that describes the hyperplane is defined as $\nabla_{\mathbf{u}} G^j \mathbf{e}'_{+i}$, which is the projection of the gradient of limit state function at the sample point onto direction $\mathbf{e}_{+i}$. Graphically, the approximation looks like fitting the limit state surface with a "box". The "box" is shown in Fig. 4.1 with black dashed lines. The limit state function is linearized not only with respect to random variables $\mathbf{u}$ but also design variables $\mathbf{x}$ at the sample points. Therefore, on each hyperplane, $\nabla_{\mathbf{u}} G$ and $\nabla_{\mathbf{x}} G$ remains constant. This segmental linearization is consistent with the idea in Eq. 4.2:

$$\begin{aligned}
\nabla_{\mathbf{x}} P_f &= -\int_S \frac{\varphi_n(\mathbf{u})}{\|\nabla_{\mathbf{u}} G\|} \nabla_{\mathbf{x}} G \mathrm{d}S \\
&\approx \sum_{j=1}^{p} \int_{S_j} -\frac{\varphi_n(\mathbf{u})}{\|\nabla_{\mathbf{u}} G\|} \nabla_{\mathbf{x}} G \mathrm{d}S_j \\
&= \sum_{j=1}^{p} -\frac{\int_{S_j} \varphi_n(\mathbf{u}) \mathrm{d}S_j}{\|\nabla_{\mathbf{u}} G^j \mathbf{e}'_{+i}\|} \nabla_{\mathbf{x}} G^j
\end{aligned} \tag{4.3}$$

where S_j is one of the planar segments which appears as a face of the "box"; p is the number of sample point (i.e. the number of planar segments). Comparing with Eq. 4.2, we can find the weight for discrete component $\nabla_{\mathbf{x}} G^j$ at j^{th} sample point simply defined by:

$$W_j = -\frac{\int_{S_j} \varphi_n(\mathbf{u}) \mathrm{d}S_j}{\|\nabla_{\mathbf{u}} G^j \mathbf{e}'_{+i}\|} \tag{4.4}$$

Then we need to integrate the integral term in Eq. (4.4). We still suppose $\mathbf{u}^{(+i)}$ is the j^{th} sample point. Using the orthogonality between adjacent planar segments and the rotational symmetry of the standard normal space, we can obtain:

$$\begin{aligned} \int_{S_j} \varphi_n(\mathbf{u}) \mathrm{d}S_j &= \varphi(\|\mathbf{u}^{(+i)}\|) \int_{S'_j} \varphi_{n-1}(\hat{\mathbf{u}}') \mathrm{d}S'_j \\ &= \varphi(\|\mathbf{u}^{(+i)}\|) \prod_{k=1, k\neq i}^{n} \left(\Phi(\|\mathbf{u}^{(+k)}\|) + \Phi(\|\mathbf{u}^{(-k)}\|) - 1\right) \end{aligned} \tag{4.5}$$

where S'_j is S_j described in the new rotated coordinates; n is the dimension of random space (i.e. number of transformed random variables). If $\mathbf{u}^{(\pm k)}$ is not a sample point, we take $\Phi(\|\mathbf{u}^{(\pm k)}\|) = \Phi(\infty) = 1$. Substituting Eq. (4.5) to Eq. (4.4), the weight can be computed as:

$$W_j = -\frac{\varphi(\|\mathbf{u}^{(+i)}\|)}{\|\nabla_{\mathbf{u}} G^j \mathbf{e}'_{+i}\|} \prod_{k=1, k\neq i}^{n} \left(\Phi(\|\mathbf{u}^{(+k)}\|) + \Phi(\|\mathbf{u}^{(-k)}\|) - 1\right) \tag{4.6}$$

The idea of using segmental linear functions to approximate nonlinear limit state surface is not novel. In [33], a so-called multi-point FORM (also named as polyhedral approximation) is addressed for approximating failure probability, which adopts locally most central points to construct a tangent bounding polyhedron of the limit state surface. Different from the multi-point FORM, the proposed segmental multi-point linearization method (SML) is developed for the purpose of sensitivity calculation. Thus, instead of bounding the limit state surface with a tangent polyhedron to get a narrow bound of failure probability, the SML interpolates the limit state function with an orthogonal "box" which leads directly to a multi-point discrete approximation of the sensitivity of failure probability. In addition, the points we choose to

construct linearization are not necessarily local or global most central points and they can be generated systematically. This allows a great flexibility in the linearization of nonlinear limit state surfaces and does not require special iterative numerical techniques for searching the local and global most central points [39]. However, in the future, as we exploring different variations of SML, the linearization scheme of multi-point FORM can be one of the possibilities.

To test the performance of the method, a simple illustrative numerical example is conducted. Consider a limit state function defined as follows:

$$G(x, u_1, u_2) = -xu_1^2 - u_2 + c \tag{4.7}$$

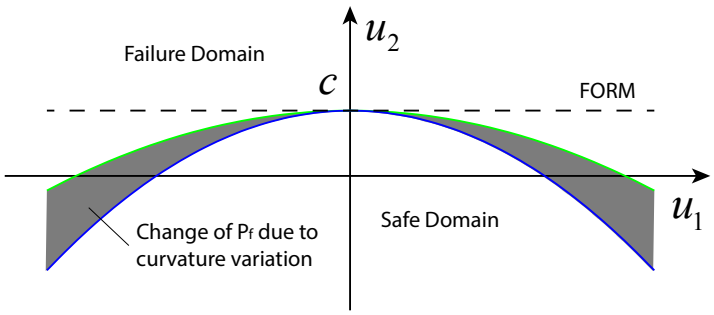

Figure 4.2: Parabolic limit state function.

where x is the design variable; u_1 and u_2 are random variables; and c is a system parameter which is the intercept of the curve $G = 0$ with axis u_2. Function G is directly defined in the standard normal random space, thus there is no need to do the transformation of random variables. The function G has also been used by Der Kiureghian and Dakessian [39] in the study of limit state surface with multiple local design points. The design variable x controls the curvature of the limit state surface. The function is properly designed such that the analytical solution for the unique design point stays at $(0, c)$ for any $x \leqslant 0.5$ and $c \geqslant 1.0$. The reliability index obtained by FORM is then $\beta_1 = c$ and corresponding approximate failure probability equals $1 - \Phi(c)$. If the FORM-based approximation is used to compute the sensitivity of P_f with respect to x, we will get:

$$\frac{\partial P_f}{\partial x} = -\frac{\varphi(\beta)}{\|\nabla_{\mathbf{u}} G^*\|}(-u_1^2)|_{u_1=0} = 0 \tag{4.8}$$

The zero here should not be interpreted as a special case. Instead, it illustrates the inability of the FORM-based approximation (i.e. Eq. (3.10)) to capture any change of probability due to variations on curvature of the limit state surface. In this example, as x changes its value, the failure domain will also change. The corresponding change in P_f can be quite significant but Eq. (4.8) would never reflect this change as shown in Fig. 4.2. Fig. 4.3 shows the normalized values of the sensitivity calculated by different methods for different values of c. The sensitivity is normalized by the failure probability obtained by FORM (i.e. $P_{f,1} = 1-\Phi(c)$) in order to demonstrate the relative importance of the sensitivity. We chose c to be 2 and 3 because they are the most commonly used target reliabilities for structural engineering. The exact solution is obtained by numerical quadrature of Eq. (3.21). This can be done since there are only two random variables and one design variable involved in this problem. In general, Eq. (3.21) is very hard to be evaluated by numerical integration. The finite difference (FD) method is performed using a central difference scheme, and $P_f(x \pm \Delta x)$ is evaluated by MCS with coefficient of variation (c.o.v.) equals 0.5%. From Fig. 4.3 one can see that the approximated sensitivity obtained by the proposed method approximates the exact value quite well. For positive curvatures (i.e. $x < 0$), the proposed method is the same with FORM-based approximation, but in this case, both of them provide good approximations of the sensitivity. The reason is that for a limit state surface with positive curvature, the change of failure domain due to change of x is located relatively far away from the origin thus the change in P_f is almost negligible. As the curvature becomes negative and the absolute value of it becomes large, the proposed method will start to make improvement while FORM-based approximation cannot provide any useful information.

4.2 Improvement of Reliability Assessment

Requiring no additional computation, the calculated weights can also be used to improve the approximation of P_f. The idea here resembles the multi-point FORM. In consistence with the "box" representation of the limit state surface, the region inside the "box" can approximates the safe domain as shown in Fig. 4.4. Due to the orthogonality between adjacent linear segments, the

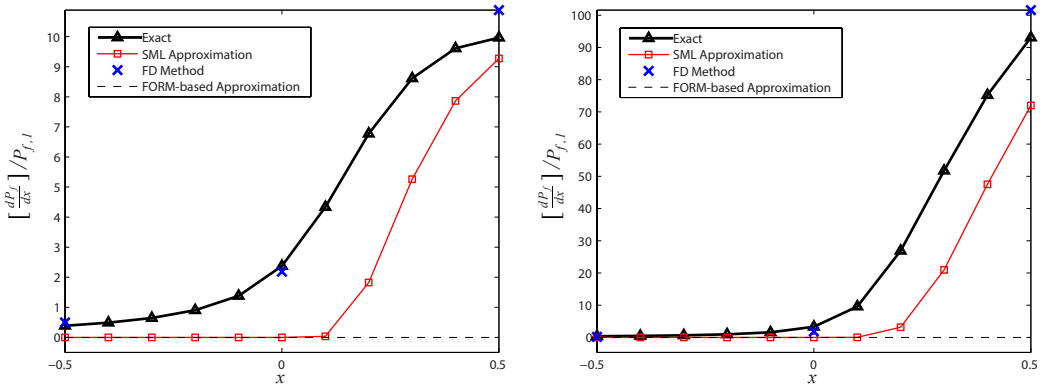

(a) $c = 2$. (b) $c = 3$.

Figure 4.3: Comparison of approximations of sensitivity.

failure probability is given by:

$$P_f = 1 - \prod_{i=1}^{n} \left(\Phi(\|\mathbf{u}^{(+i)}\|) + \Phi(\|\mathbf{u}^{(-i)}\|) - 1 \right) \tag{4.9}$$

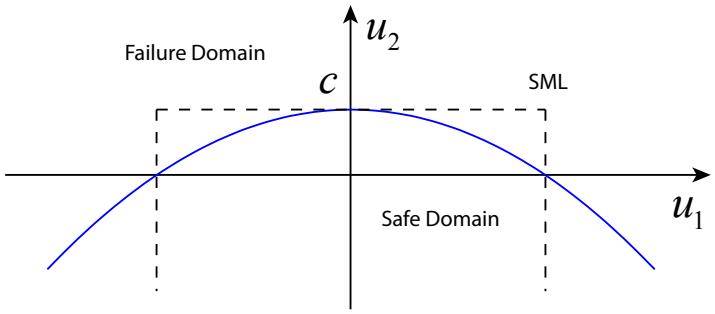

Figure 4.4: SML for parabolic limit state surface.

If the design point is taken as the reference point, the above expression can be regarded as a modification of traditional FORM approximated P_f. The obtained P_f will be larger or equal to the P_f obtained by traditional FORM. It turns out to improve FORM when FORM underestimates the failure probability; it will provide same value with FORM when FORM makes a fairly good approximation or when FORM is conservative.

This simple scheme is applied to the limit state function in previous section to examine its accuracy. Fig. 4.5 shows the failure probability obtained by FORM, SML, SORM and MCS. The MCS is performed with c.o.v equals to 2.5%. The SORM approximation is based on Breitung's formula (see Section 3.1). The result shows that SML is better than FORM and even comparable

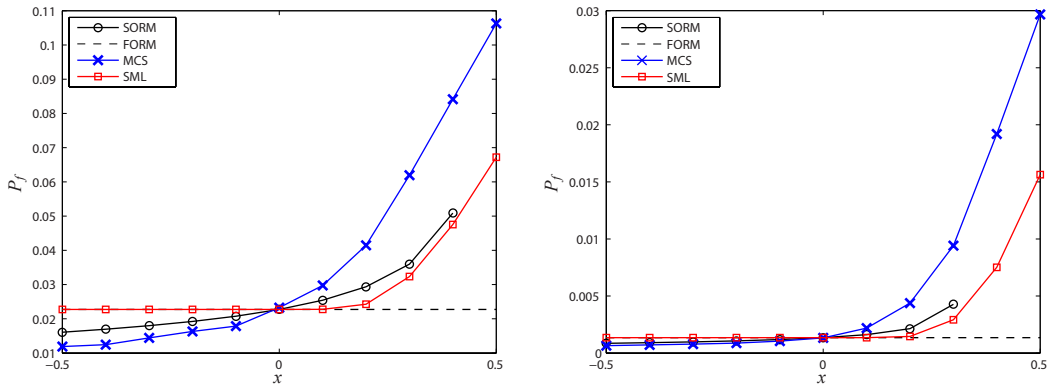

(a) $c = 2$. (b) $c = 3$.

Figure 4.5: Comparison of approximations of failure probability.

with SORM. A problem with SORM is that it will not be valid for limit state surfaces with large negative curvature [32].

In this Chapter, we only consider that the origin is inside the safe domain. However, for the case that the origin is in the failure domain, one can use the scheme to approximate the probability of safety (i.e. P_s) and the sensitivity of safe probability (i.e. $\nabla_{\mathbf{x}} P_s$), and then use the equality $P_f = 1 - P_s$ to get P_f and $\nabla_{\mathbf{x}} P_f$.

4.3 SML-Based RBTO Algorithm

In this section, we are going to discuss how to apply the SML method in optimization process and how to choose and adjust the optimizer.

Since the sensitivity is calculated by combining the information from multiple points for the SML, the optimization process becomes naturally more stable and robust than the traditional approaches using one-point discrete approximation of sensitivity. Because there is only one point used to calculate the sensitivity, if the point (i.e. $\mathbf{u}^*$ for RIA or $\mathbf{u}^t$ for PMA) change its location rapidly, the traditional approaches may suffer huge jumps in the calculated sensitivity. However, for a SML-based approach, even though the sample points could be quite different among different iterations, the weighted sum of sensitivity approximation would stay relative stable in value since the weights are calculated adaptively. Actually, we have a quite large flexibility in choosing the reference point. The reference point is not required to be

dominating, so it can be any point that is on the limit state surface or even just near the surface. This allows a single loop scheme to be possible. A rigorous search for the reference point at each iteration is not required even if the design point is set to be the reference point. We can use the existing procedures in single loop RBDO methods to get the approximated design point [23, 24, 20, 21, 16]. In this work, we adopt an incomplete improved HL-RF search to get the design point. The location of the design point is updated simultaneously with the design variables by using the updating formula of improved HL-RF algorithm within one step of the topology optimization iteration and recycling the data as the starting point for next iteration. Similar strategy that is based on original HL-RF algorithm can be found in [20]. The design point is suggested to be the reference point due to two reasons:

1. It is the closest point on the limit state surface to the origin, thus the information at the design point is of the most importance if neglecting the effect of the denominator, $\|\nabla_{\mathbf{u}} G\|$, in Eq. (3.21);

2. Taking the design point as the reference point makes sure that the algorithm convert to FORM-based algorithm when the limit state function does not have a large negative curvature.

However, it is not restricted to use the design point as reference point. As an example of other possible reference point, one can specify a particular direction that the reference point has to be on and solve a 1-D nonlinear equation to get the reference point that is on the limit state surface. Additionally, heuristic update of the approximated P_f is also possible. As implemented in other RBDO algorithms [19, 25], SORM, MCS or other reliability methods can be used to get a more precise failure probability rather than using the SML for reliability analysis as described in previous section.

The optimizer used in this research is the Method of Moving Asymptotes (MMA) [40], which is quite popular for structural optimization. It turns out that some other popular nonlinear programming techniques, namely Sequential Linear Programming (SLP) and Convex Linearization Method (CONLIN), are special cases of MMA [40, 15]. Thus one advantage of using MMA is that it provides a unified library of some popular programming methods, and we can make choices just by adjusting the artificial parameters. The MMA code used in this research is a simplified version of MMA which is

specially developed for compliance-volume optimization in the book by Klarbring and Christensen [15]. The general code of MMA written by Svanberg is used as a reference. In our implementation, as we adjust the parameter to achieve and improve convergence, we finally make the MMA method equivalent to CONLIN. In our experiments, CONLIN works very well for topology optimization with probabilistic constraint. The CONLIN method was developed by Fleury which is published one year earlier than MMA in 1986 [41], and it is now rarely used in DTO because of its slow convergence. The reason for its slow convergence is that the method makes a too conservative convex approximation of the original problem [15]. Thus for a convex optimization problem like the nested formulation, the convergence will turn out to be slow. However, for RBTO which is not a convex optimization in most cases, a conservative approximation is indeed preferred. Intuitively, when doing RBTO, as the design variables being updated, the limit state surface in the random space also varies. For most RBTO methods, including the proposed one, they use discrete point(s) to track the change of limit state surface, which requires an update of the point(s) at each iteration as well. If the design variables changes too fast, the numerical method may not be able to update the point(s) correctly to capture the change of limit state surface especially for single loop approaches. Since the problem is not convex, the optimization can easily diverge due to an error in one step of iteration.

Even though CONLIN tends to make conservative updates, we can still observe some oscillatory behavior. To eliminate the oscillations, an adaptive limiter on step size is added to the updating scheme. Optimizers like CONLIN and MMA will calculate the value of design variables for next iteration directly instead of calculating a step like most other optimizers do, so our updating scheme appears as follows:

$$\mathbf{x}^{k+1} = \alpha(\bar{\mathbf{x}}^{k+1} - \mathbf{x}^k) + \mathbf{x}^k \tag{4.10}$$

where k is the current step number; $\bar{\mathbf{x}}^{k+1}$ is the output of the optimizer; α is the adaptive step size which is defined as:

$$\alpha = \begin{cases} c_{fast} & \text{if } \operatorname{sgn}(x_i^k - x_i^k) = \operatorname{sgn}(\bar{x}_i^{k+1} - x_i^k) \\ c_{slow} & \text{if } \operatorname{sgn}(x_i^k - x_i^k) \neq \operatorname{sgn}(\bar{x}_i^{k+1} - x_i^k) \end{cases} \tag{4.11}$$

The two parameters c_{slow} and c_{fast} controls the step size. The limiter is ap-

plied to each design variables. When a member keep increasing or decreasing its size during the optimization process, it should be safe to make a relatively large step size (i.e. c_{fast}); in contrast, when a member size oscillates, we should use a smaller step size (i.e. c_{slow}) to limit the potential of divergence. The choice of c_{fast} and c_{slow} depends on specific problem. In general, they work well with the setting $c_{fast} = 0.6$ and $c_{slow} = 0.1$. This heuristic method works effectively as we perform the RBTO problems. Although as a trade-off, more number of iterations is needed to converge, for most problems, we can get smooth convergence other than divergence or oscillation.

CHAPTER 5

NUMERICAL EXAMPLES

5.1 A Benchmark Problem

The first example for RBTO is a benchmark problem proposed by Rozvany [42]. The analytical solution for the problem has been derived. It can be used to check the validity of numerical methods for RBTO. The problem is depicted in Fig. 5.1a. The design domain has a width $L = 2$ and depth $D = 1$. The horizontal force H is the only random variable. H is characterized by a normal distribution with a mean of 0 and a standard deviation of 1. The vertical force V is fixed with a value of 3 acting downwards. Young's modulus E is taken as a unit value. The formulation of the optimization problem is described in Section 5. The threshold for the compliance is $C^{max} = 1$. The target failure probability is 0.0027, which corresponds to $\beta_t = 2.7822$, as proposed in [42].

The analytical solution of the problem is given by a two-bar truss as shown in Fig. 5.1b with $\alpha = 35.26439°$ and a non-dimensional volume of 2.44949. The non-dimensional volume is defined as V/AL, where A is the

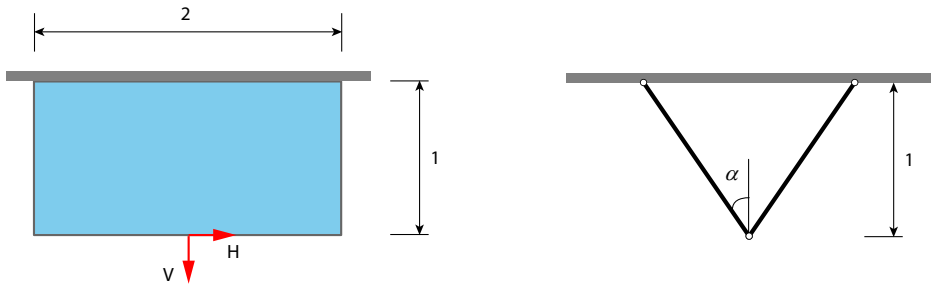

(a) (b)

Figure 5.1: Benchmark problem for RBTO. (a) Domain, loading and boundary conditions. (b) Optimal topology.

cross-sectional area of the members and L is the width of the design domain. The numerical solution by the proposed algorithm is extracted from a ground structure on a 40×2 grid with full connectivity, which results in 4322 non-overlapping potential members in total. The obtained topology is almost the same with the analytical solution. It has an angle $\alpha = 34.9920$ and non-dimensional volume of 2.4530. The difference is mainly due to the discrete nature of the ground structure approach.

Some FORM-based methods can also provide correct answer to the problem [24]. However, our new method achieves the optimum in a more reasonable way. For this benchmark problem, it is clear that there are two symmetric design points. One corresponds to H towards left and the other refers to the case when H is acting to the right. As discussed before, most of the FORM-based algorithms would calculate the sensitivity at only one point in the random space. Therefore, the optimal structure is actually designed for either H to the left or to the right but not both. The only reason that a correct result can be obtained is because linear elastic material behaves the same in tension and compression, so the direction of H does not really matter in this particular case. While the SML-based algorithm proposed in this thesis takes a combination of derivatives evaluated at both design points and the optimization is performed considering both H to the left and right. Therefore, even though the proposed method does not show its advantage in this benchmark problem, it is more logically rational and computationally robust in general. The advantage will be demonstrated in detail in following examples.

5.2 Symmetric Crane Arm Design

In this example, we are going to demonstrate the advantage of the new method by comparing the results of DTO, FORM-based PMA and the proposed SML-based RIA. The objective is to minimize the volume of the structure with a probabilistic constraint described in terms of compliance. Consider a crane arm design in a domain shown in Fig. 5.2. The topology optimization is performed on a 9×3 ground structure with level 6 nodal connectivity in horizontal direction and level 3 in vertical direction as shown in Fig. 5.3. The material of the structure is linear elastic with Young's

Modulus $E = 100$. The structure is subjected to two independent vertical loads acting on the two tips of the crane. Each of them is assumed to follow a normal distribution with mean of 7.0 and standard deviation of 3.0. The limit on compliance is set to be $C^{max} = 1.2$. Since there are only two random variables involved, we can plot the limit state surface in a 2-D plot in order to compare the obtained optimal designs in detail.

First, a DTO is conducted. The two loads take their mean values multiplied by a safety factor of 2. The obtained optimal design is shown in Fig. 5.4. The members are plotted with thickness proportional to computed member areas. The volume of the structure is 96 (rounded off). However, this topology of structure is not stable. It is a common issue of DTO that it can provide optimal topology of structure that is not stable. Due to the small lower bound of the members in nested formulation of the ground structure approach, the optimal structure still has a little bit of resistance to collapse in its computational model. The actual failure probability is then measured to be 0.96 by a Monte Carlo simulation with c.o.v. equals 2.5%. In the rest of the thesis, the actual failure probabilities are all refers to the result obtained by MCS since the c.o.v. is set to be small and the obtained failure probability is very close to the true value.

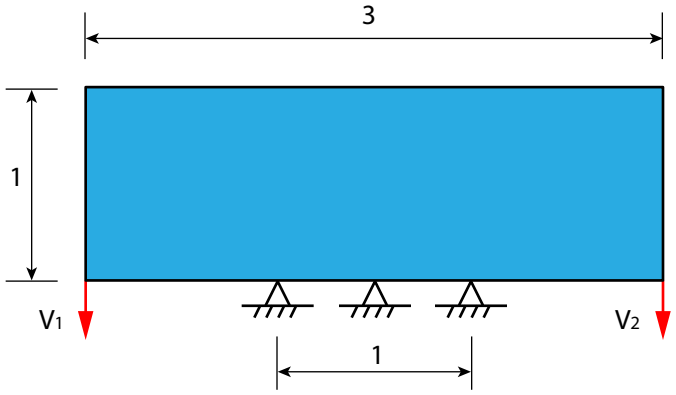

Figure 5.2: Design domain and boundary conditions of example 2.

Next, a FORM-based RBTO is perform using a single loop PMA. The target failure probability is $P_f^t = 0.0013$ which corresponds to a target reliability index of 3.0. Fig. 5.5 shows the obtained optimal design. The result has an optimal volume equals 89 and actual $P_f = 0.6554$. The contour plot of compliance function is plotted in Fig. 5.7. The thick curve is the limit

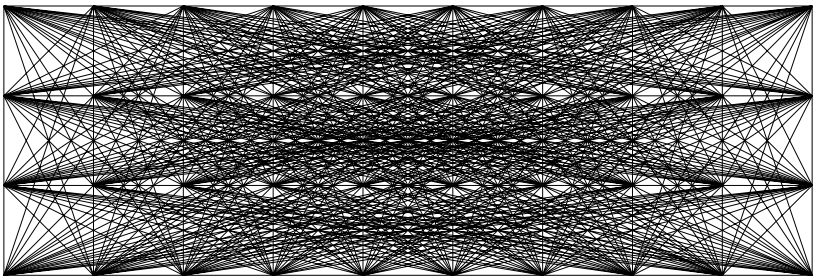

Figure 5.3: Ground structure used to do RBTO which has 440 non-overlapping members.

state surface of $G = 0$ in the standard normal random space, where u_1 and u_2 are the transformed random variables of the vertical force V_1 and V_2. We can see that the MPP which is expected to be the design point of final design converges to a point that is a local maximum point with respect to $\|\mathbf{u}\|$. This happens with single loop methods, since they use the solution of the KKT necessary conditions of Eq. (3.12) to replace the thorough search for $\mathbf{u}^t$. The MPP in blue circle in Fig. 5.7 satisfies the necessary conditions but is not the expected $\mathbf{u}^t$. The invalid design is obtained because of a cumulation of error in sensitivity calculation during the optimization process. With different settings of initial point for $\mathbf{u}^t$, we may get different optimal topologies, for example the one shown in Fig. 5.7. If double loop PMA, which we also tried, is used, the optimization will not be able to converge. Same thing happens with double loop RIA. This is due to the fact that the initial design has a limit state function that are symmetric about the line $u_1 = u_2$ in the random space, thus either the $\mathbf{u}^*$ in RIA or $\mathbf{u}^t$ in PMA will oscillate between two points as the structure been optimized either for the case $V_1 > V_2$ or $V_1 < V_2$. Similar behavior of FORM-based gradient methods for RBTO with density approach is reported in the paper by Silva *et al* [24].

The SML-based algorithm is then performed to the problem. We consider two variations of the algorithm: (1) set the reference point to be the design point; (2) enforce the reference point to be in the direction of $u_1 = u_2$, which corresponds to $V_1 = V_2$. The optimal structural layout obtained by formulation (1) is presented in Fig. 5.8 and the result by (2) is shown in Fig.

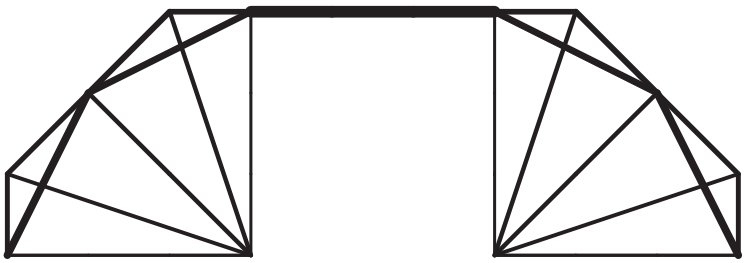

Figure 5.4: Optimal topology by DTO.

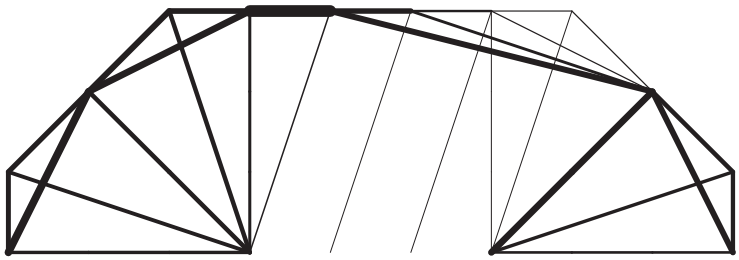

Figure 5.5: Optimal topology by FORM-based PMA.

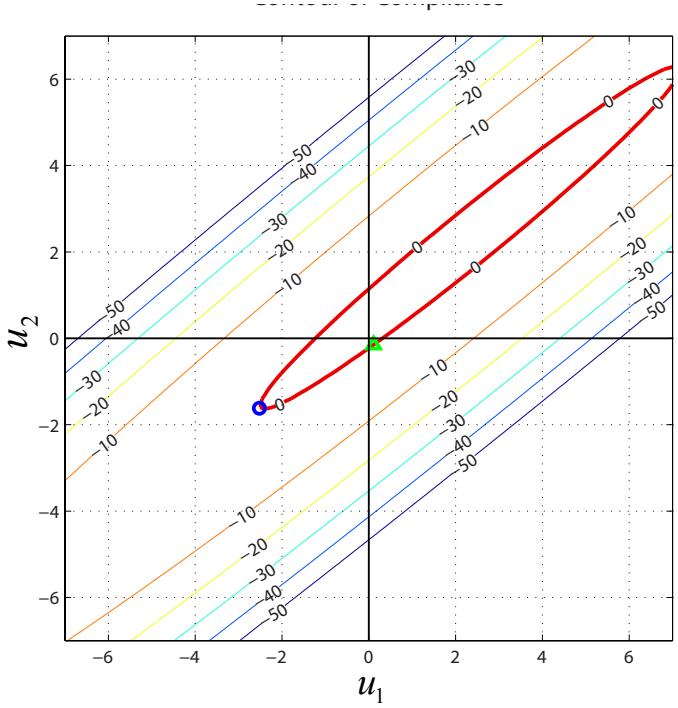

Figure 5.6: Contour plot of $G(\mathbf{u}, \mathbf{x}^*)$ for optimal design of Fig. 5.5. The blue circle indicates the design point computed by the PMA; the green triangle refers to the actual position of design point; the red solid curve is the limit state surface described by $G(\mathbf{u}, \mathbf{x}^*) = 0$.

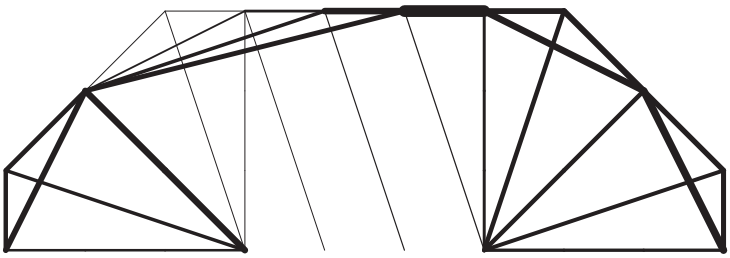

Figure 5.7: Another optimal topology by FORM-based PMA.

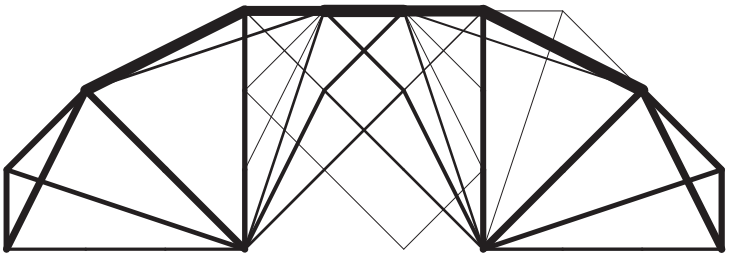

Figure 5.8: Optimal topology by SML-based RIA taking design point the reference point.

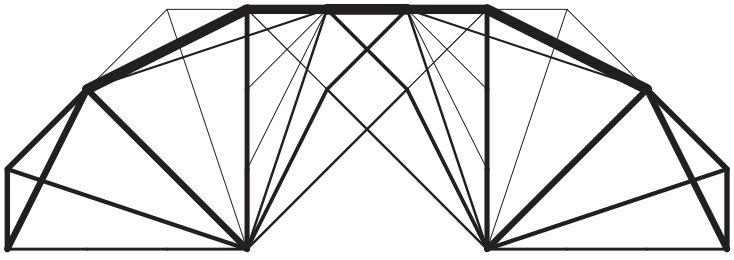

Figure 5.9: Optimal topology by SML-based RIA enforcing reference point to be on the line $u_1 = u_2$.

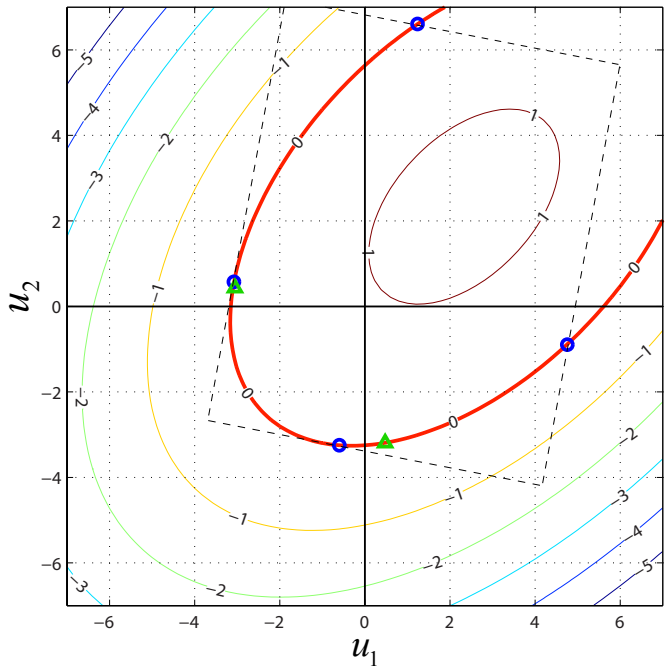

Figure 5.10: Contour plot of $G(\mathbf{u}, \mathbf{x}^*)$ for optimal design of Fig. 5.8. The blue circle indicates the sample points; the green triangle refers to the design point(s); the green triangle refers to the actual position of design point; the red solid curve is the limit state surface described by $G(\mathbf{u}, \mathbf{x}^*) = 0$.

5.9. The two results are very similar, the first one has an optimal volume equals 121 with actual reliability index of 2.8 and the second one has a volume of 114 and reliability index of 2.7. In terms of safe probability (i.e. $1 - P_f$), the errors are 0.13% and 0.22% compare to the target reliability 0.9987. The design loads and domain are all symmetric thus the optimal topology should also be symmetric. However, the first one is close to a symmetric design but not exactly symmetric. By specifying the direction of reference point, the second one converges to a symmetric optimal design because the reference point is on the symmetry axis of the limit state function, which makes the symmetry of initial design being preserved. The example shows that the choice of reference point is quite flexible, and we can make our choices to get desired features, for example symmetric topology as in this example. Fig. 5.10 and Fig. 5.11 are the contour plots of the limit state functions for the obtained optimal designs. Taking the design point as the reference point results in 4 sample points. The safe region is approximated by a closed

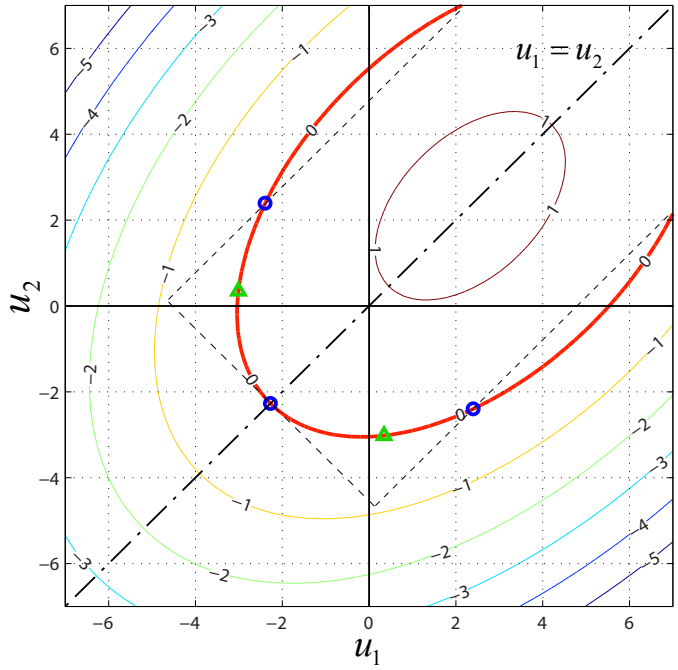

Figure 5.11: Contour plot of $G(\mathbf{u}, \mathbf{x}^*)$ for optimal design of Fig. 5.9. The blue circle indicates the sample points; the green triangle refers to the design point(s); the green triangle refers to the actual position of design point; the red solid curve is the limit state surface described by $G(\mathbf{u}, \mathbf{x}^*) = 0$.

"box" as shown in dashed lines in both figures. The second form yields 3 sample points, and they are symmetric about the line $u_1 = u_2$. The "box" is not closed and the limit state surface is approximated by three segments. Although none of the two design points is captured, we still get a good approximation of the sensitivity.

5.3 Unsymmetric Crane Arm Design

In the previous example, the FORM-based methods cannot provide a valid design. Furthermore, We will show that even in the case that the FORM-based RBTO algorithm could provide valid design, the design may not be optimal. In this example, the design domain is modified to be unsymmetric. The design domain is now a 4 by 1 rectangle with the loads still on the two tips but not symmetric about support (see Fig. 5.12). The ground structure

used to do the optimization is a 12×3 grid with level 6 nodal connectivity which contains 629 non-overlapping members. The target reliability index is set to be 2.0. which is equivalent to have $P_f^t = 0.0228$. The Young's modulus E, limitation on compliance C^{max}, vertical forces V_1 and V_2 are the same with the previous example. The PMA used in the last example is performed as a representation of the FORM-based methods.

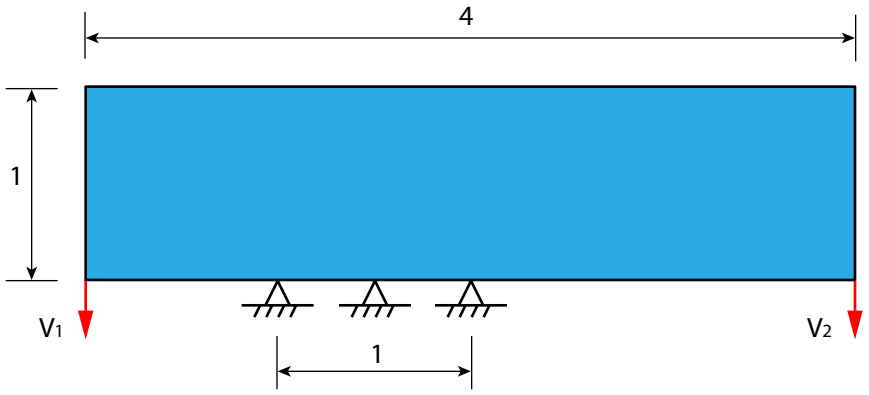

Figure 5.12: Design domain and boundary conditions of example 3.

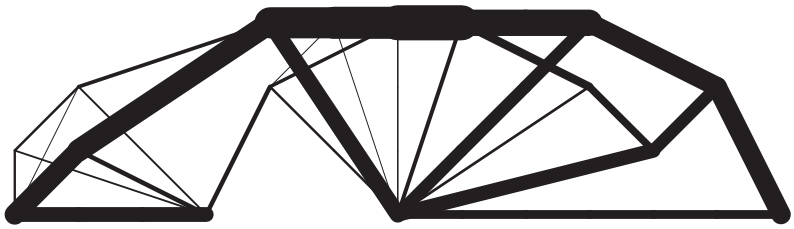

Figure 5.13: Optimal topology by DTO.

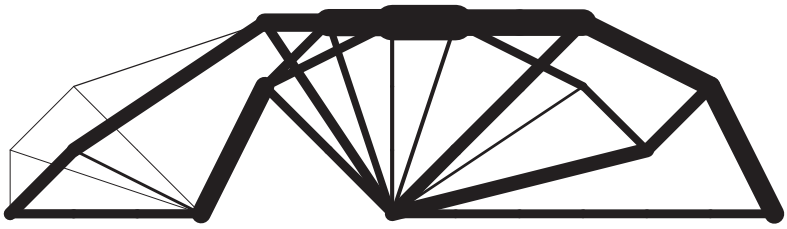

Figure 5.14: Optimal topology by FORM-based PMA.

DTO is also performed with a safety factor of 2 (see Fig. 5.13). The optimal topology by DTO is stable for this problem with a volume of 286, but as we test the design by MCS, the reliability index is only 1.04. Fig.

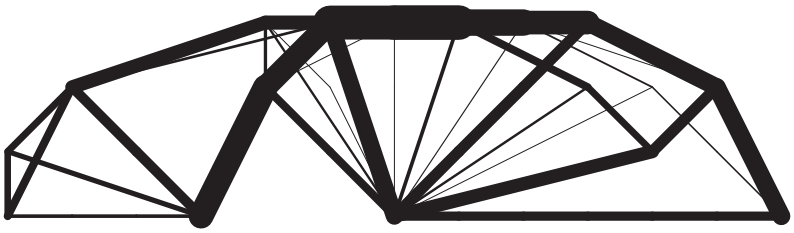

Figure 5.15: Optimal topology by SML-based RIA with design point being the reference point.

5.14 shows the optimal topology obtained by the PMA. For this problem, the MPP $\mathbf{u}^t$ successfully converges to the unique design point of the final design. The result has a volume equals 274 and the actual reliability index is 1.5. Unlike its performance in the previous example, the obtained design is valid. However, comparing to the design obtained by the new approach (as shown in Fig. 5.15), the design by SML-based RIA is closer to the optimal design than FORM-based single loop PMA. The proposed new method converges to a design with volume of 278 and a reliability index, obtained by MCS, of 1.9. The two designs are almost same in volume but the design by SML-based approach has a higher reliability, which means that the material is assigned more efficiently by the proposed algorithm than the conventional FORM-based algorithm. Although we cannot prove rigorously that the new method converges to a global optimum, we can still conclude that the new approach provides a better result than the traditional method. The error in sensitivity makes the numerical solution of FORM-based algorithms not close to the real optimum that satisfies the KKT conditions. The contour plot of the limit state function of the design obtained by SML-based algorithm is shown in Fig. 5.16. We can see that the reference point coincides with the design point of the final design. This reference point generates 3 sample points in total.

To incorporate the randomness in material property, we add the Young's modulus as an additional random variable which has a lognormal distribution with a mean of 100 and a standard deviation of 10. The lognormal distribution is employed because it cannot have a negative value, which matches the physical nature of Young's modulus. The PDF of E is plotted in Fig. 5.17. The optimal design has a volume equals 286 and actual reliability index of 1.9. Comparing to the design with a fixed E, the volume increases due to

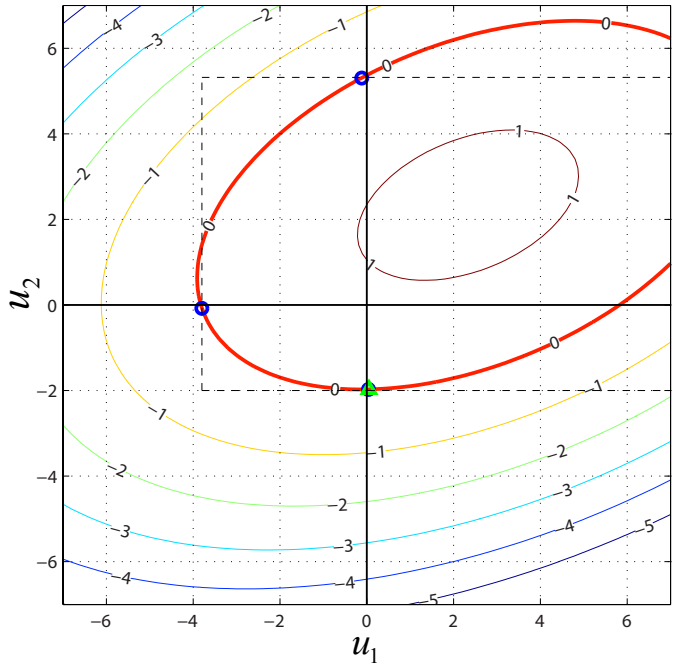

Figure 5.16: Contour plot of $G(\mathbf{u}, \mathbf{x}^*)$ for optimal design of Fig. 5.15. The blue circle indicates the sample points; the green triangle refers to the design point; the red solid curve is the limit state surface described by $G(\mathbf{u}, \mathbf{x}^*) = 0$.

the introduction of uncertainty in material property. The optimal topology is presented in Fig. 5.18, which is also slightly different with the one without considering randomness of E.

5.4 T-shaped Building Design

The final example is a comprehensive design problem towards potential realistic applications. We are going to design the structural components of a T-shaped building as shown in Fig. 5.19a. The design domain has a concave geometry rather than a simple rectangle. This is to show that the algorithm is universally suitable to handle arbitrary design domains. The design domain can be generated by the algorithm developed by Zegard and Paulino which is based on restriction zone method [12]. The ground structure used to perform the optimization is shown in Fig. 5.19b. The structure carries two vertical loads (V_1 and V_2), and two horizontal loads H_1 and H_2. The four

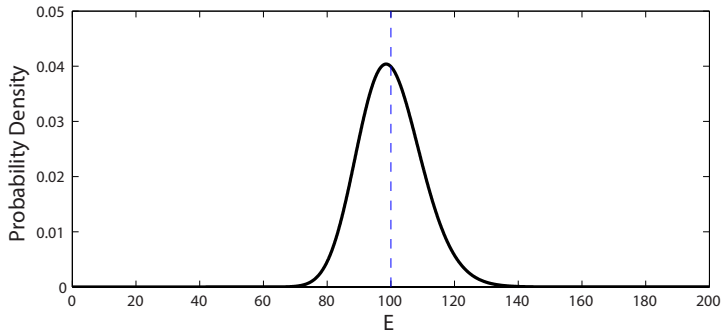

Figure 5.17: Probability distribution of Young's modulus E.

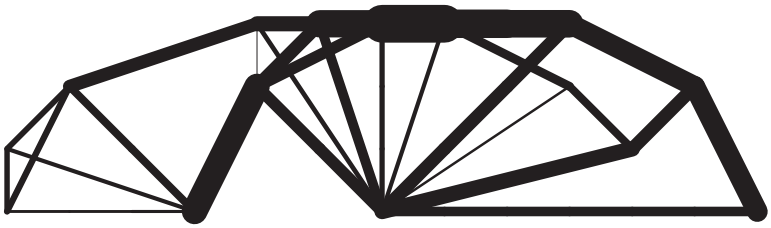

Figure 5.18: Optimal topology by SML-based RIA considering randomness of E.

forces and Young's modulus are taken as random variables in this problem. The probability distributions of the random variables can be found in Table. 5.1. The building is fixed at the bottom. Unlike the previous examples, the random variables in this problem are not independent to each other. V_1 and V_2 are correlated with a correlation coefficient (C.C.) of 0.2; H_1 and H_2 have a correlation coefficient of 0.7. This makes the problem more practical.

Table 5.1: Statistics of Random Variables for Example 4.

Variable	Distribution Type	Mean	Standard Deviation	C.C.
V_1	Normal	-5	2	0.2
V_2	Normal	-5	2	
H_1	Normal	0	3	0.7
H_2	Normal	0	3	
E	Lognormal	100	10	0.0

The DTO provides a result shown in Fig. 5.20. The magnitude of loads are the mean values multiplied by a safety factor of 2. The design has an optimal volume equals 225. However, it is nearly an unstable structure.

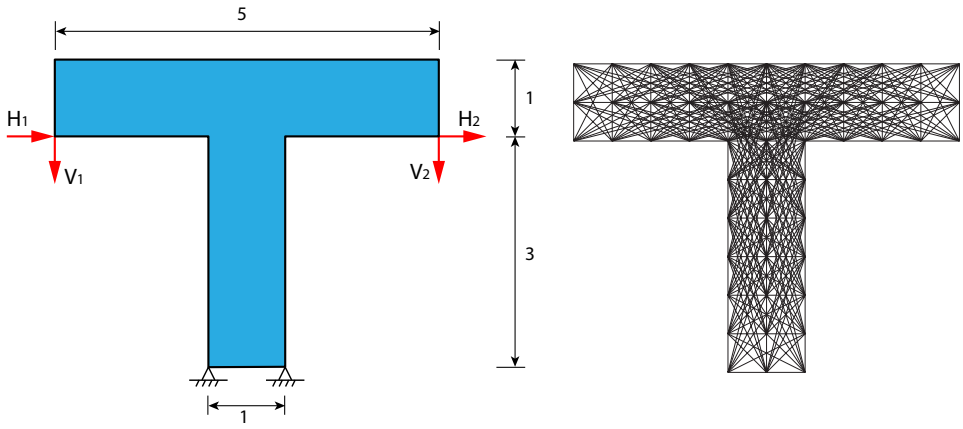

(a) (b)

Figure 5.19: T-shaped building design. (a) Domain, loading and boundary conditions. (b) Ground structure used to perform RBTO which contains 526 non-overlapping members.

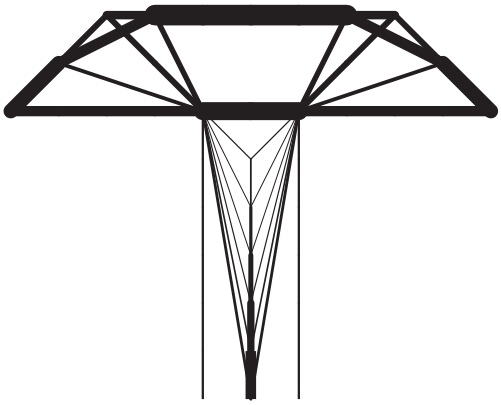

Figure 5.20: Optimal topology by DTO.

The problem is also performed with the single loop PMA used in previous examples. However, the algorithm fails to converge. Fig. 5.21 shows the optimal design considering uncertainties in load and material property by SML-based RIA with target reliability index of 3.0. The reference point is set to be in the direction of $[1, 1, 0, 0, 0]$ as the vector of random variables denoted in the order of $[V_1, V_2, H_1, H_2, E]$. Employing the SML-based RIA, the optimal design is computed to have an optimal volume of 582. The actual failure probability measured by MCS equals 0.006, which corresponds to a reliability index of 2.51. As we increase the number of potential members, we can get a refined optimal topology. The topology shown in Fig. 5.22 is

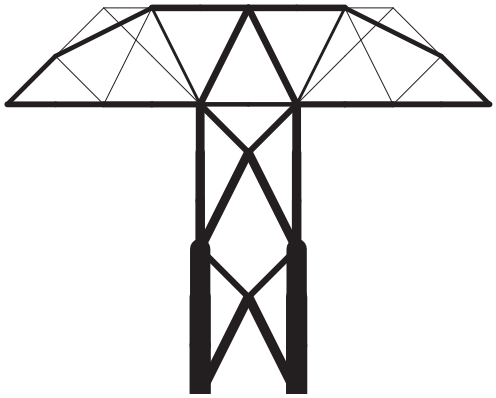

Figure 5.21: Optimal topology by SML-based RIA on the ground structure shown in Fig. 5.19b.

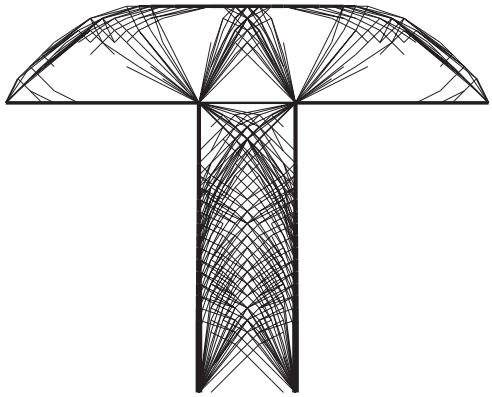

Figure 5.22: Optimal topology by SML-based RIA on a refined ground structure with 26180 members.

extracted from a ground structure with 26180 bars. The volume of structure and reliability is almost the same as the one in Fig. 5.21 with only the volume decreasing by 2. The members shown are not plotted proportional to computed member areas in order to make sure that the details can be better presented. Although the refined topology may not be very useful for structural design since it is hard to construct, it could provide useful information about the analytical solution of BRTO problems.

CHAPTER 6

CONCLUDING REMARKS AND SUGGESTIONS FOR FUTURE WORK

The random nature and uncertain variation of design conditions can tremendously affect how we design a structure. The deterministic topology optimization techniques which are formulated without consideration of the intrinsic uncertainty and randomness in structural design problems may cause the optimal design to be impractical in real circumstances.

Reliability based topology optimization provides a balance between economy and reliability of a structural design. In this thesis, a RBTO algorithm is proposed for truss layout design problems with uncertainties in design. The algorithm adopts the segmental multi-point linearization method to improve the approximation of failure probability and its sensitivity with respect to design variables. The SML-based algorithm is more suitable for RBTO problems with nonlinear limit state functions than conventional FORM-based algorithms that are adopted without considering the special property of topology optimization.

Several examples are conducted considering uncertainties in loading conditions and material property (Youngs modulus for linear elastic design). The optimal designs obtained by the proposed method are generally closer to the true optimum than the result obtained by DTO or other FORM-based algorithms because the SML-based algorithm approximates the KKT conditions better. In the cases that the traditional methods cannot converge or cannot converge to a valid design, the SML-based algorithm is more numerically robust and stable as it can converge to a valid optimum. It is also worth to notice that the proposed method reduces to the traditional FORM-based RIA automatically when the limit state function is linear or nearly linear if the design point is selected to be the reference point. In addition, as a single loop gradient-based algorithm the computational efficiency of the algorithm is quite attractive as compared to other methods based on large number of simulations for example the model updating approach. Structural engineers

should find the obtained solutions reasonable and useful because the grid-based nature of ground structure approach allows the resultant truss layout to be used in structural design without too much effort on abstracting useful information from the optimal topology.

6.1 Contributions

1. Pointed out that for RBTO problems, the conventional FORM-based algorithms may not be suitable;
2. Introduced the integral form of gradient of failure probability to RBDO;
3. Developed a SML method for sensitivity calculation of probabilistic constraint and reliability analysis in reliability-based optimization;
4. Proposed an efficient optimization algorithm based on SML for RBTO on ground structures.

6.2 Suggestions for Future Work

1. Explore variations of the SML method, for example SML with different linearization schemes;
2. Implement the SML-based algorithm to solve 3-D RBTO problems, for example realistic design of buildings and bridges;
3. Generalize the SML-based algorithm to solve RBDO problems with non-linear limit state functions.

REFERENCES

[1] G. Rozvany, "Aims, scope, methods, history and unified terminology of computer-aided topology optimization in structural mechanics," *Structural and Multidisciplinary Optimization*, vol. 21, no. 2, pp. 90–108, 2001.

[2] M. Bendsøe and O. Sigmund, *Topology Optimization: Theory, Methods and Applications*. Springer, 2003.

[3] A. Sutradhar, G. H. Paulino, M. J. Miller, and T. H. Nguyen, "Topological optimization for designing patient-specific large craniofacial segmental bone replacements," *Proceedings of the National Academy of Sciences*, vol. 107, no. 30, pp. 13 222–13 227, 2010.

[4] G. Schüeller and H. Jensen, "Computational methods in optimization considering uncertainties an overview," *Computer Methods in Applied Mechanics and Engineering*, vol. 198, no. 1, pp. 2 – 13, 2008.

[5] M. Schevenels, B. Lazarov, and O. Sigmund, "Robust topology optimization accounting for spatially varying manufacturing errors," *Computer Methods in Applied Mechanics and Engineering*, vol. 200, no. 4952, pp. 3613 – 3627, 2011.

[6] J. Zhao and C. Wang, "Robust topology optimization under loading uncertainty based on linear elastic theory and orthogonal diagonalization of symmetric matrices," *Computer Methods in Applied Mechanics and Engineering*, vol. 273, no. 0, pp. 204 – 218, 2014.

[7] S. Mathakari, P. Gardoni, P. Agarwal, A. Raich, and T. Haukaas, "Reliability-based optimal design of electrical transmission towers using multi-objective genetic algorithms," *Computer-Aided Civil and Infrastructure Engineering*, vol. 22, no. 4, pp. 282–292, 2007.

[8] D. Greiner and P. Hajela, "Truss topology optimization for mass and reliability consiationsco-evolutionary multiobjective formulations," *Structural and Multidisciplinary Optimization*, vol. 45, no. 4, pp. 589–613, 2012.

[9] W. Achtziger, M. Bendsøe, A. Ben-Tal, and J. Zowe, "Equivalent displacement based formulations for maximum strength truss topology design," *IMPACT of Computing in Science and Engineering*, vol. 4, no. 4, pp. 315 – 345, 1992.

[10] A. Ben-Tal and M. Bendsøe, "A new method for optimal truss topology design," *SIAM Journal on Optimization*, vol. 3, no. 2, pp. 322–358, 1993.

[11] T. Sokół, "A 99 line code for discretized michell truss optimization written in mathematica," *Structural and Multidisciplinary Optimization*, vol. 43, no. 2, pp. 181–190, 2011.

[12] T. Zegard and G. Paulino, "GRAND - ground structure based topology optimization for arbitrary 2D domains using MATLAB," *Structural and Multidisciplinary Optimization*, pp. 1–22, 2014.

[13] C. Talischi, G. Paulino, A. Pereira, and I. Menezes, "PolyTop: A Matlab implementation of a general topology optimization framework using unstructured polygonal finite element meshes," *Structural and Multidisciplinary Optimization*, vol. 45, no. 3, pp. 329–357, 2012.

[14] B. Topping, "Mathematical programming techniques for shape optimization of skeletal structures," in *Shape and Layout Optimization of Structural Systems and Optimality Criteria Methods*, ser. International Centre for Mechanical Sciences, G. Rozvany, Ed. Springer Vienna, 1992, vol. 325, pp. 349–375.

[15] P. Christensen and A. Klarbring, *An Introduction to Structural Optimization*, ser. Solid Mechanics and Its Applications. Springer, 2008.

[16] J. Tu, K. K. Choi, and Y. H. Park, "Design Potential Method for Robust System Parameter Design," *AIAA Journal*, vol. 39, pp. 667–677, Apr. 2001.

[17] J. Royset, A. Kiureghian, and E. Polak, "Reliability-based optimal design of series structural systems," *Journal of Engineering Mechanics*, vol. 127, no. 6, pp. 607–614, 2001.

[18] J. Royset, A. Kiureghian, and E. Polak, "Reliability-based optimal structural design by the decoupling approach," *Reliability Engineering & System Safety*, vol. 73, no. 3, pp. 213 – 221, 2001.

[19] J. Royset, A. Der Kiureghian, and E. Polak, "Optimal design with probabilistic objective and constraints," *Journal of Engineering Mechanics*, vol. 132, no. 1, pp. 107–118, 2006.

[20] G. Cheng, L. Xu, and L. Jiang, "A sequential approximate programming strategy for reliability-based structural optimization," *Computers and Structures*, vol. 84, no. 21, pp. 1353 – 1367, 2006.

[21] J. Liang, Z. P. Mourelatos, and E. Nikolaidis, "A single-loop approach for system reliability-based design optimization," *Impact of Computing in Science and Engineering*, vol. 129, no. 12, pp. 1215 – 1224, 2007.

[22] M. McDonald and S. Mahadevan, "Design optimization with system-level reliability constraints," *Journal of Mechanical Design*, vol. 130, no. 2, pp. 021 403–1 – 021 403–10, 2008.

[23] T. H. Nguyen, J. Song, and G. H. Paulino, "Single-loop system reliability-based design optimization using matrix-based system reliability method: Theory and applications," *Journal of Mechanical Design*, vol. 132, no. 1, pp. 011 005–1 – 011 005–11, 2010.

[24] M. Silva, D. Tortorelli, J. Norato, C. Ha, and H.-R. Bae, "Component and system reliability-based topology optimization using a single-loop method," *Structural and Multidisciplinary Optimization*, vol. 41, no. 1, pp. 87–106, 2010.

[25] T. H. Nguyen, J. Song, and G. H. Paulino, "Single-loop system reliability-based topology optimization considering statistical dependence between limit-states," *Structural and Multidisciplinary Optimization*, vol. 44, no. 5, pp. 593–611, 2011.

[26] K. Mogami, S. Nishiwaki, K. Izui, M. Yoshimura, and N. Kogiso, "Reliability-based structural optimization of frame structures for multiple failure criteria using topology optimization techniques," *Structural and Multidisciplinary Optimization*, vol. 32, no. 4, pp. 299–311, 2006.

[27] J. Royset and E. Polak, "Reliability-based optimal design using sample average approximations," *Probabilistic Engineering Mechanics*, vol. 19, no. 4, pp. 331 – 343, 2004.

[28] M. Jalalpour, T. Igusa, and J. K. Guest, "Optimal design of trusses with geometric imperfections: Accounting for global instability," *International Journal of Solids and Structures*, vol. 48, no. 21, pp. 3011 – 3019, 2011.

[29] A. Michell, "The limits of economy of material in frame structures," *Philosophical Magazine*, vol. 8, no. 47, pp. 589–597, 1904.

[30] M. Ohsaki, *Optimization of Finite Dimensional Structures*. Taylor & Francis, 2010.

[31] S. Choi, R. Grandhi, and R. Canfield, *Reliability-based Structural Design*. Springer, 2006.

[32] R. Rackwitz, "Reliability analysisa review and some perspectives," *Structural Safety*, vol. 23, no. 4, pp. 365 – 395, 2001.

[33] O. Ditlevsen and H. Madsen, *Structural Reliability Methods*. Technical University of Denmark, 2007.

[34] A. Hasofer and N. Lind, *An Exact and Invariant First-order Reliability Format*. Solid Mechanics Division, University of Waterloo, 1973.

[35] Y. Zhang and A. D. Kiureghian, "Two improved algorithms for reliability analysis, reliability and optimization of structural systems," in *Proceedings of the Sixth IFIP WG7. 5 Working Conference on Reliability and Optimization of Structural Systems*, Assisi, Italy, 1995, pp. 297–304.

[36] K. Breitung, "Asymptotic approximations for probability integrals," *Probabilistic Engineering Mechanics*, vol. 4, no. 4, pp. 187 – 190, 1989.

[37] M. Hohenbichler and R. Rackwitz, "Sensitivity and importance measures in structural reliability," *Civil Engineering Systems*, vol. 3, no. 4, pp. 203–209, 1986.

[38] S. Uryasev, "Derivatives of probability functions and integrals over sets given by inequalities," *Journal of Computational and Applied Mathematics*, vol. 56, no. 12, pp. 197 – 223, 1994.

[39] A. D. Kiureghian and T. Dakessian, "Multiple design points in first and second-order reliability," *Structural Safety*, vol. 20, no. 1, pp. 37 – 49, 1998.

[40] K. Svanberg, "The method of moving asymptotes - a new method for structural optimization," *International Journal for Numerical Methods in Engineering*, vol. 24, no. 2, pp. 359–373, 1987.

[41] C. Fleury and V. Braibant, "Structural optimization: A new dual method using mixed variables," *International Journal for Numerical Methods in Engineering*, vol. 23, no. 3, pp. 409–428, 1986.

[42] G. Rozvany, "Exact analytical solutions for benchmark problems in probabilistic topology optimization," in *EngOpt2008-international conference on engineering optimization*, Rio de Janeiro, Brazil, 2008.